Diesel fuel spray penetration, heating, evaporation and ignition: modelling vs. experimentation

S.S. Sazhin*

Sir Harry Ricardo Laboratories,
Internal Combustion Engines Group,
School of Environment and Technology,
University of Brighton,
Brighton BN2 4GJ, UK
E-mail: S.Sazhin@brighton.ac.uk
*Corresponding author

S.B. Martynov

Department of Mechanical Engineering,
University College London,
Torrington Place, London, WC1E 7JE, UK
E-mail: s_martynov@meng.ucl.ac.uk

T. Kristyadi

Mechanical Engineering Department,
National Institute of Technology of Bandung,
Jl. PHH Mustofa no. 23, Bandung, Indonesia
E-mail: kristyadi@itenas.ac.id

C. Crua and M.R. Heikal

Sir Harry Ricardo Laboratories,
Internal Combustion Engines Group,
School of Environment and Technology,
University of Brighton,
Brighton BN2 4GJ, UK
E-mail: C.Crua@brighton.ac.uk
E-mail: M.R.Heikal@brighton.ac.uk

Abstract: The modified WAVE droplet breakup model, taking into account the transient processes during spray injection, the Effective Thermal Conductivity (ETC) liquid phase model, the gas phase model suggested by Abramzon and Sirignano, and the customised version of the Shell autoignition model have been implemented into the KIVA 2 CFD code. The observed Diesel spray tip penetration and Sauter Mean Radii show much better agreement with the prediction of the modified WAVE model compared with other droplet breakup models. The difference in the autoignition delay times predicted using the Infinite Thermal Conductivity (ITC) and ETC models is important for practical computations.

Keywords: diesel fuel spray; droplet breakup; heating; evaporation; autoignition.

Reference to this paper should be made as follows: Sazhin, S.S., Martynov, S.B., Kristyadi, T., Crua, C. and Heikal, M.R. (2008) 'Diesel fuel spray penetration, heating, evaporation and ignition: modelling vs. experimentation', *Int. J. Engineering Systems Modelling and Simulation*, Vol. 1, No. 1, pp.1–19.

Biographical notes: Sergei Sazhin is Professor of Thermal Physics at the University of Brighton (UK). He completed his PhD Degree (Physics and Mathematics) at St. Petersburg State University (Russia) in 1977. Fellow of the Institute of Physics, a Chartered Physicist. Research Worker, Institute of Physics, St. Petersburg State University, Russia (1972–1982); research fellow, Department of Physics, Sheffield University, UK (1988–1992); research scientist, Fluent Europe Ltd., Computational Fluid Dynamics Software and Consultancy Services, Sheffield, UK (1992–1996). Since 1996, he has been researching the modelling of fluid dynamics, heat transfer and combustion processes in internal combustion engines at the University of Brighton.

Sergey Martynov joined University College London (UK) as a Research Fellow in 2007. He completed his PhD degree at the University of Brighton in 2005 and his BSc and MSc

degrees in Physics at the Moscow Power Engineering Institute (Russia) in 1996 and 1998 respectively. Researcher at the Institute of High Temperatures (Moscow) between 1996 and 2002. Research Fellow at the University of Brighton, studying the nature of breakup in sprays in direct injection Diesel engines, between 2005 and 2007. His current research interests are focused on the theoretical characterisation of coated microbubbles for ultrasound diagnostic imaging and therapy.

Tarsisius Kristyadi is Lecturer in the Mechanical Engineering Department of the Institute of Technology in Bandung (Indonesia). He completed his PhD degree at the University of Brighton (UK) in 2007, Masters and undergraduate degrees at the Mechanical Engineering Department of the Institute of Technology in Bandung (Indonesia) in 2000 and 1996 respectively. He was trained in Gas Engines in 2001 and Pumps and Turbo machinery in 1998 (both at the Institute of Technology in Bandung). Author of 18 research papers, including four papers in international refereed journals.

Cyril Crua obtained his PhD in 2002 for his experimental studies of Diesel spray atomisation, combustion and soot formation. He has supervised five PhD students who studied advanced Diesel combustion strategies for ultra-low emissions, the modelling of Diesel atomisation, as well as developing state-of-the-art laser diagnostic techniques. He is now responsible for the management and funding of the diesel research within the ICEG at the University of Brighton. His current research work includes the development and application of advanced laser diagnostics techniques for the measurement of in-cylinder spray atomisation and pollutants formation.

Morgan R. Heikal is Professor of Thermofluids, Leader of the IC Engines Research Group and Deputy Head of the School of Environment and Technology at the University of Brighton. He completed his PhD degree in Heat Transfer at UMIST (Manchester) in 1976. He is Fellow of the Institution of Mechanical Engineers, Member of EPSRC Peer Review College, Member of Scientific Council of the International Centre for Heat and Mass Transfer, Member of Society of Automotive Engineers Transactions Selection Committee, Member of Combustion Engines and Fuels Group IMechE since 1999 and Visiting Engineer, Ricardo UK since 1998.

1 Introduction

The importance of accurate multi-dimensional modelling of the processes in Diesel engines and Diesel engine-like environments is well recognised (Flynn et al., 1999; Bertoli and na Migliaccio, 1999; Sazhina et al., 2000; Zhou et al., 2006; Wang and Rutland, 2007). This modelling needs to take into account a number of complicated fluid dynamics, heat/mass transfer and combustion processes in a realistic three-dimensional combustion chamber configuration. This inevitably leads to the application of rather simplistic models describing individual processes. These include simplistic chemical models, droplet breakup models which do not take into account transient effects, and droplet heating models which disregard the effects of internal temperature gradient, and so on. The aim of this paper is to investigate the necessity for and feasibility of relaxing some of these simplifying assumptions referring to the modelling of droplet breakup, heating and evaporation. This analysis will be based on the customised version of the KIVA 2 Computational Fluid Dynamics (CFD) code, in which more realistic models of these processes have been implemented. The results of validation of this code against in-house experimental data will be presented and discussed.

Various conventional droplet breakup models, used in CFD codes, are briefly reviewed in Section 2. In the same section, a further development of one of these models, taking into account jet acceleration, is discussed. The most straightforward way of validating these models seems to be the comparison of the spray penetration predicted by them with available experimental data. The relevant results are presented and discussed in Section 3. These results refer to relatively low gas temperatures when the effects of droplet heating and evaporation on spray dynamics can be ignored. Recent developments in droplet heating and evaporation models are briefly summarised in Section 4. The customised version of the Shell autoignition model used in our calculations is described in Section 5. The experimental set-up used for the validation of the models is described in Section 6. The test cases used for the comparison with the predictions of the customised version of the KIVA 2 code are briefly described in Section 7. Results of the comparison of predicted and experimental results are presented and discussed in Section 8. The main results of the paper are summarised in Section 9.

2 Droplet breakup models

The Lagrangian approach to spray modelling, based on the description of droplets at a sub-grid scale, is generally more popular than the Eulerian one (Nijdam et al., 2006). It is implemented in an open-source non-commercial

computer code KIVA 2, widely used for development and validation of spray models (Amsden et al., 1989; Reitz and Rutland, 1995). One of the most important elements of Lagrangian spray models is focused on jet and droplet breakups. The nature of the breakup process depends on a spray region. Primary breakup takes place near the nozzle exit. Here disintegration of the liquid jet takes place. In the far-field spray, where the liquid phase is dispersed in the gas, the secondary breakup of large droplets into smaller ones takes place (Faeth et al., 1995). In many practical applications, unified models have been used both for primary and secondary breakups. In these models, the jet is approximated by a chain of droplets, with initial diameters equal to the diameter of the nozzle, or slightly less than this diameter if the effects of cavitation are taken into account. For implementation into CFD codes, designed for computation of three-dimensional sprays, the so called Taylor Analogy Breakup (TAB) and WAVE models of breakup and their modifications are commonly applied (Stiesch, 2003). The TAB model describes the breakup of liquid droplets using an analogy with a spring-mass system (O'Rourke and Amsden, 1987). The WAVE model is based on the results of linear stability analysis of the gas-liquid interface at a jet surface (Reitz, 1987). This model and its later modifications have been widely applied for computation of liquid sprays (Patterson and Reitz, 1998; Beale and Reitz, 1999; Kong et al., 1999). An important limitation of the above mentioned breakup models relates to the fact that they are based on an unrealistic assumption about single-size droplets created after the breakup. More realistic stochastic models describe the breakup in terms of the evolution of the droplet distribution function over time. One of these models, suitable for implementation into CFD codes, was developed by Gorokhovski and Saveliev (2003). This model takes into account the stochastic nature of the secondary breakup at high Weber numbers, and is useful for predictions for a wide spectra of droplets in sprays (Gorokhovski and Saveliev, 2003; Apte et al., 2003).

Another limitation of the conventional breakup models stems from an assumption about quasi-steady-state flow conditions, although in many practical applications spray injection is an essentially transient process. For example, in modern Diesel engines, fuel is injected during a very short time, when the rate of injection continuously increases in response to the needle lift inside the injector (Russel et al., 2000). When describing these sprays using conventional models, it is generally assumed that temporal variations of the injection velocity do not affect the stability and breakup of the liquid-gas interface. The effect of acceleration on the breakup of a liquid jet was studied by Domann and Hardalupas (2004). However, the analysis described in this paper was performed assuming the steady-state injection condition and ignoring the initial stage of the jet formation. This assumption is acceptable for modelling relatively slow sprays, but it is not at first evident in the case of highly transient sprays. Computations described by Kaario et al. (2002) and Sarre et al. (1999), using the above mentioned WAVE and TAB breakup models, showed that the spray penetration can be significantly under-predicted during the initial stage of injection. This could be related to the fact that these models ignore the effect of injection acceleration on spray breakup.

In what follows, the main features of the conventional TAB, WAVE and stochastic models are briefly described. Then a modification of the conventional WAVE model, taking into account the effect of jet acceleration, is discussed.

2.1 Conventional WAVE model

The WAVE model, originally developed by Reitz (1987), is based on the analysis of the Kelvin-Helmholtz instability of a liquid jet. This instability leads to stripping of child droplets from the liquid core. The core is approximated by parent droplet parcels injected from the nozzle. The radii of the droplets in these parcels (R_d) continuously decrease during the breakup process, as described by the following equation:

$$\frac{\mathrm{d}R_d}{\mathrm{d}t} = -\frac{R_d - R_{d(\mathrm{eq})}}{t_{bu}}, \tag{1}$$

where t_{bu} is the characteristic breakup time, $R_{d(\mathrm{eq})}$ is the radius of equilibrium (stable) droplets:

$$R_{d(\mathrm{eq})} = \begin{cases} B_0\Lambda, & B_0\Lambda \le R_d \\ \mathcal{R}, & B_0\Lambda > R_d, \end{cases} \tag{2}$$
$$\mathcal{R} = \min\begin{pmatrix} (3\pi R_d^2 U/(2\Omega))^{0.33} \\ (3R_d^2\Lambda/4)^{0.33}, \end{pmatrix}$$

$B_0 = 0.61$ is the model constant, Λ and Ω are the wave length and the frequency of the fastest growing disturbance on the surface of a liquid jet, U is the jet velocity. The breakup time t_{bu} is estimated as:

$$t_{bu} = 3.726\, B_1 \frac{R_d}{\Lambda\,\Omega}. \tag{3}$$

The breakup constant B_1 was taken equal to 10 based on the results of measurements of quasi-steady-state Diesel spray penetration at relatively low injection pressures (Hiroyasu and Kadota, 1974). Later, the WAVE model was extensively tested for computation of transient Diesel sprays, and it was shown that the breakup constant B_1 can vary widely depending on the type of injector used (Reitz and Rutland, 1995).

The further development of the WAVE model took into account the effect of the Rayleigh–Taylor (RT) instability of droplets (Patterson and Reitz, 1998). The wavelength corresponding to the maximal increment of this instability is given by the expression $\Lambda_{RT} = 2\pi\sqrt{3\sigma_s/(a_{RT}\rho_l)}$, where σ_s is the surface tension, $a_{RT} = \frac{3}{8}C_D\frac{\rho_g U^2}{\rho_l R_d}$, C_D is the drag coefficient, ρ_g and ρ_l are densities of gas and liquid, respectively. When Λ_{RT} is less than the diameter of a droplet, breakup is expected to take place. In this case $R_{d(\mathrm{eq})}$ is calculated as $C_{RT}\Lambda_{RT}$, where $C_{RT} = 2.5$ is the

model constant (Patterson and Reitz, 1998). The breakup time is estimated as:

$$t_{bu\,\mathrm{RT}} = \sqrt{\frac{3}{2a_{RT}}\sqrt{\frac{3\sigma_s}{\rho_l\, a_{RT}}}}.$$

Kelvin–Helmholtz instability is mainly responsible for the primary breakup, while the Rayleigh–Taylor mechanism prevails at the secondary atomisation stage (Patterson and Reitz, 1998; Beale and Reitz, 1999).

2.2 TAB model

The Taylor Analogy Breakup (TAB) model describes the process in terms of the critical deformation of an oscillating-distorting droplet (O'Rourke and Amsden, 1987). The external force is caused by the relative drop motion, the restoring force is the surface tension force, and the damping term results from the liquid viscosity. It is assumed that breakup occurs when the droplet deformation exceeds $R_d/2$. The Sauter Mean Radius (SMR) of the product droplets at the moment of breakup is found from the conservation of droplet energy during the breakup process:

$$\mathrm{SMR} = \frac{R_d}{\frac{7}{3} + \frac{\rho_l R_d v_{\mathrm{def}}}{4\sigma_s}},$$

where R_d is the parent droplet radius, v_{def} is the velocity of droplet deformation at the moment of breakup.

In contrast to the WAVE model, in the TAB model, after breakup, the product droplets' radii $R_{d\,\mathrm{pr}}$ follow the distribution:

$$f(R_{d\,\mathrm{pr}}) = \frac{1}{\overline{R}}\exp\left(-\frac{R_{d\,\mathrm{pr}}}{\overline{R}}\right),$$

where $\overline{R} = \mathrm{SMR}/3$ is the number averaged product droplet radius.

The spray penetration predicted by the TAB model agrees with the results of measurements by Hiroyasu and Kadota (1974). At the same time it over-predicts the rate of droplet breakup, and tends to predict smaller droplets close to the injector (cf. Tanner, 2004). Despite the above mentioned problems, the TAB model is widely used for spray computations, and it is a default breakup model in the KIVA 2 code.

2.3 Stochastic model

As follows from the previous analysis, the WAVE model is essentially a deterministic model, in which the radii of product droplets are determined by equation (2). The TAB model has a stochastic element in choosing the radii of product droplets assuming that the distribution function of these droplets is *a priori* given, but it still focuses on sample droplets rather than on the whole spectrum. The model suggested by Gorokhovski and Saveliev (2003) is based on a completely different approach to breakup modelling. Their approach is based on the assumption, originally suggested by Kolmogorov (1941), that the breakup of parent particles into secondary particles does not depend on the instantaneous sizes of the parent particles. This assumption is obviously not valid when R_d is close to $R_{d(\mathrm{eq})}$. In high pressure injection sprays, characterised by large Weber numbers, the hydrodynamic mechanism of atomisation due to the mean velocity difference at the liquid-gas surface, can be complicated by the impact of turbulent fluctuations on jet breakup (Gorokhovski and Saveliev, 2003). Under such conditions, when the specific mechanism of atomisation and the scale of the breakup length cannot be clearly defined, stochastic approaches to the modelling of breakup become more appropriate than deterministic ones.

It was shown by Gorokhovski and Saveliev (2003) that in the limit of large times $t \to \infty$, the general equation for the evolution of the droplet number distribution function $F(R_d)$ can be presented in the form of the Fokker–Planck type equation:

$$\frac{\partial F(R_d)}{\partial t} = \left[-3\langle\ln\alpha\rangle - \frac{9}{2}\langle\ln^2\alpha\rangle - \frac{\partial}{\partial R_d}R_d\langle\ln\alpha\rangle + \frac{1}{2}\frac{\partial}{\partial R_d}R_d\frac{\partial}{\partial R_d}R_d\langle\ln^2\alpha\rangle\right]\nu F(R_d), \qquad (4)$$

where

$$\langle\ln^n\alpha\rangle = \int_0^1 \ln^n\alpha\, q(\alpha)\,\mathrm{d}\alpha,$$

$\alpha \in [0,1]$ is the parameter linking the radii of product (R_d) and parent (R_{d0}) droplets ($\alpha = R_d/R_{d0}$), $q(\alpha)\mathrm{d}\alpha$ is the normalised probability that the radius of each product droplet is within the range $[\alpha R_d,\ (\alpha+\mathrm{d}\alpha)R_d]$, $\nu = \nu_0 q_0$, ν_0 is the breakup frequency of an individual droplet, q_0 is the average number of droplets produced after each breakup action.

Equation (4) depends on two unknown constants $\langle\ln\alpha\rangle$ and $\langle\ln^2\alpha\rangle$. To reach an agreement between the predictions of this model and the measurements by Hiroyasu and Kadota (1974), it was assumed that $\langle\ln\alpha\rangle = -1/2$ and $\langle\ln^2\alpha\rangle = 1$. The frequency of breakup ν was obtained from the relation:

$$\nu = \frac{1}{B_1}\frac{|U|}{R_{d0}}\sqrt{\frac{\rho_g}{\rho_l}}. \qquad (5)$$

The value of constant $B_1 = \sqrt{3}$ was chosen in order to match experimental data on the stripping breakup of droplets.

The above described models have mostly been validated for quasi-steady-state sprays, injected at constant or slowly varying velocities. However, to the best of our knowledge, the effect of unsteady injection at the initial stage of formation of Diesel spray has not been addressed in the literature, and none of the above models have been tested specifically for this transient period of injection. In the next subsection a possible generalisation of one of these models (WAVE model), to take into account the transient effects during spray formation, is described.

2.4 Modified WAVE model

In order to account for the transient nature of injection on breakup, the parameters of the WAVE model, controlling the rate of spray disintegration, have been modified. The decrease in Ω with increasing injection acceleration is taken into account, while it is assumed that the wave length of critical instability Λ is not affected by the transient nature of the flow. At a qualitative level, the decrease in Ω with increasing injection acceleration can be related to the observation that flow acceleration is expected to lead to relaminarisation of the flow and thickening of the boundary layer in the gas phase around the jet for a certain range of Reynolds numbers (Narasimha and Sreenivasan, 1979). The increase in the boundary layer thickness is, in turn, expected to stabilise the gas-liquid interface (Lozano et al., 2001). This implies suppression of instability by flow acceleration. Since $t_{bu} \sim 1/\Omega$, the effect of flow acceleration is accounted for by modifying the expression for B_1 in equation (3). The following relationship is suggested:

$$B_1 = B_{1\,\mathrm{st}} + c_1 \left(a^+\right)^{c_2}, \tag{6}$$

where

$$a^+ = 2\sqrt{\mathrm{Re}}\frac{R_d}{U_{\mathrm{inj}}^2}\frac{\mathrm{d}U_{\mathrm{inj}}}{\mathrm{d}t}$$

is the acceleration parameter taking into account the effect of flow acceleration; c_1 and c_2 are adjustable constants. In the steady-state limit a^+ is zero and $B_1 = B_{1\,\mathrm{st}}$. Following Reitz (1987), we assume that $B_{1\,\mathrm{st}} = 10$. The acceleration parameter a^+ is constructed by analogy with the local pressure gradient parameter p^+ suggested by Cebeci and Smith (1974), assuming the laminar-type dependence of the local skin friction coefficient on the Reynolds number.

In order to describe the propagation of disturbances along the liquid core, we use a rigid body concept, which is an additional assumption of the model. This concept states that parcels constituting the liquid core experience no drag from the gas and move as a rigid jet at a velocity equal to the instantaneous injection velocity $U = U_{\mathrm{inj}}$. This concept is based on the experimental observation that the momentum of the core of a Diesel spray is conserved (Schugger et al., 2000) and the above mentioned observation regarding the initial spray tip velocity. In order to describe the continuous structure of the liquid core in the spray, the collision algorithm by O'Rourke (1981) has been modified; the droplets constituting the liquid core are allowed to move together during the injection acceleration stage, even when these droplets are distributed over several computational cells. According to this algorithm, an increase in the injection velocity at the nozzle, caused by injection acceleration, is immediately translated to all the droplets in the liquid core. This method naturally accounts for incompressibility of liquid, and eliminates the grid dependence of the results. In the region downstream of the spray breakup length, droplet collisions are described following O'Rourke (1981).

3 Spray penetration in 'cold' air

The droplet breakup models described in the previous section are expected to have an effect on spray heating and evaporation processes, and ultimately on the timing of the fuel vapour/air mixture autoignition. This will be discussed in Section 8. In a realistic Diesel engine-like environment the effect of these models is obscured by the contribution of other models, including those of droplet heating/evaporation and chemical autoignition. Hence, to identify the most suitable droplet breakup model we found it appropriate to perform the testing of these models in a 'cold' gas environment, before considering realistic Diesel engine-like conditions.

The predictions of the models described in Section 2 have been compared with the results of in-house measurements of Diesel fuel sprays. Comparisons were performed for sprays injected through a single-hole nozzle of 0.2 mm in diameter into compressed air at temperature 572 K and pressure 4 MPa. Spray penetration data were obtained from the analysis of video recordings, combined with the mass flow rate measurements (Karimi et al., 2006). Based on the measured mass flow rate, the average velocity of injection was calculated. The results are shown in Figure 1. As can be seen from this figure, the observed spray is highly transient and we anticipate that the modified WAVE model, described in Section 2.4, is the most appropriate one for its analysis.

Figure 1 Calculated instantaneous jet injection velocities. A single-hole injector with nozzle diameter 0.2 mm was used. The injector and in-cylinder pressures were 160 MPa and 4 MPa respectively. The ambient gas temperature was estimated as 572 K

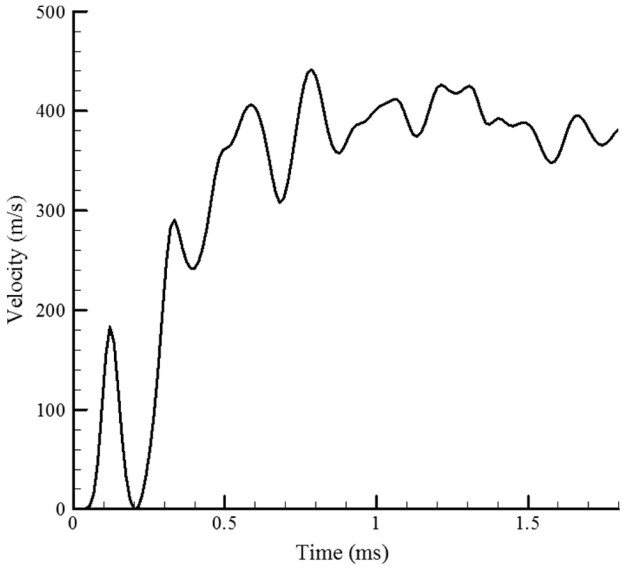

Spray computations were performed using the KIVA 2 code, in which the models described in Section 2 have been implemented (Amsden et al., 1989). Droplet parcels were injected into a cylindrical gas-filled domain using the blob injection method. Spray computations were performed in two dimensions, taking into account the

observed axial symmetry of the flow. The flow domain was represented by a constant volume gas chamber of 2 cm in radius and 10 cm in length, neglecting the piston motion during the injection pulse. The domain was covered by a uniform 2-dimensional grid, typically with 20 cells in the radial and 48 cells in the axial directions (the effects of the grid on the results will be discussed later in Section 7). The calculations were performed using all four droplet breakup models described in Section 2.

The results of calculations of spray tip penetration, using the conventional TAB and WAVE (with $B_1 = 10$), modified WAVE and stochastic models, and the corresponding experimental data are shown in Figure 2. As follows from this figure, the conventional WAVE model, TAB and stochastic models under-predict significantly the penetration at the initial stage of this process. The increase of the parameter B_1 from 10 to 60 leads to some improvement in the accuracy of the prediction of the conventional WAVE model. At the same time the modified version of the WAVE model, described in Section 2.4, gives much better agreement between the predictions of the model and experimental data, as expected, remembering the highly transient nature of the spray under consideration.

Figure 2 Experimentally observed and computed spray tip penetration. The experimental conditions were the same as in Figure 1. The computations were performed using the customised version of the KIVA 2 CFD code in which various droplet breakup models were implemented. These include the conventional TAB and WAVE (with $B_1 = 10$) models, the stochastic model and the modified WAVE model

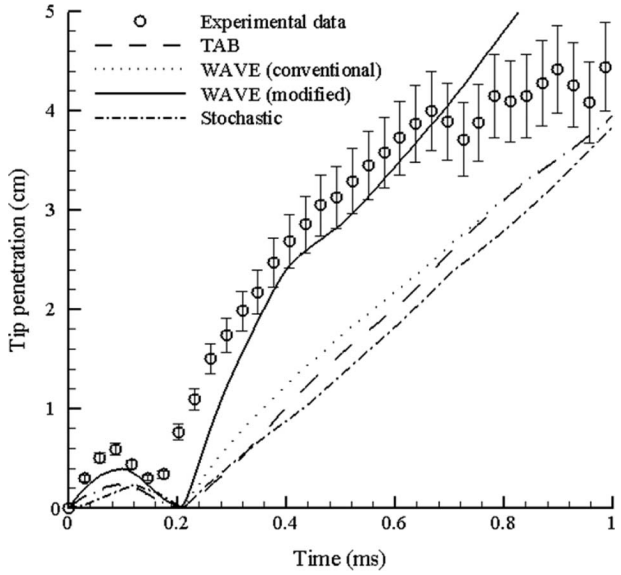

At a later stage in the injection, the cluster shedding from the tip of the spray was experimentally observed. This led to fluctuation of the observed tip penetration length at around 4 cm (see Figure 2). This phenomenon has not been addressed in the present study. In our computations, the spray penetration length was identified as the distance from the nozzle to the leading droplet parcel. This leads to the deviation between the predictions of all models and experimental data being at times 0.6 ms or greater. We anticipate that the actual tip penetration length is larger than that shown in Figure 2, as the spray at distances greater than about 4 cm from the nozzle is not actually detected by the available equipment as it is outside the optical window. Note, that in the case of spray injected into 'hot' air, the ignition takes place about 2 ms after the start of injection (Crua, 2002). For this late stage of injection, measurements of droplet size were performed for the same spray by Lacoste (2005). Figure 3 shows the experimentally observed evolution of the Sauter Mean Radius (SMR) of droplets on the spray axis (a) and its periphery (b) at a distance of 3 cm downstream from the nozzle (Lacoste, 2005). On the same figure, the results of calculations of SMR at the same locations, using the models described in Section 2, are shown. As follows from this figure, the modified WAVE model leads to the best agreement between calculated and experimental results. Although this conclusion was obtained for 'cold' sprays, we anticipate that it remains valid for more realistic 'hot' sprays. Hence, we can recommend this model for the modelling of both 'hot' and 'cold' highly transient sprays.

The models for droplet heating/evaporation and autoignition which are applicable for simulation of realistic 'hot' sprays are discussed in the next two sections.

Figure 3 Experimentally observed and computed Sauter Mean Radii (SMR) of droplets at two different locations in the spray. The models used and the experimental conditions were the same as in the case shown in Figure 2

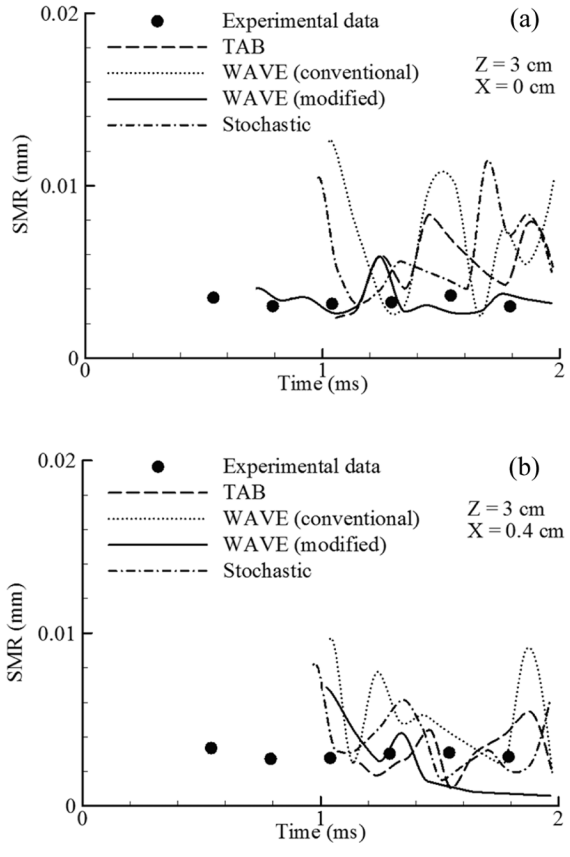

4 Droplet heating and evaporation

During the heating and evaporation of droplets, the processes in liquid and gas phases are, in general, closely linked. This has been demonstrated by coupled solutions of the heat conduction equation in these phases for stationary, spherical and non-evaporating droplets (Cooper, 1977; Sazhin et al., 2007a). However, the generalisation of this type of solution to the case of moving, evaporating droplets in a realistic environment, modelled by computational fluid dynamics codes, seems not to be feasible at the moment. Fortunately, in many practical applications, including those in Diesel engines, the diffusivity of the gas phase is substantially (more than an order of magnitude) larger than that of the liquid phase (Sazhin, 2006). This allows us to separate the processes of these phases, taking into account that gas adjusts to changing parameters much more quickly than liquid. If the initial stage (a few μs in the case of Diesel fuel droplet heating (Sazhin et al., 2001)) is ignored then it can be assumed that the heating of droplets by the gas phase can be described in terms of a steady-state heat transfer coefficient. This assumption, universally used in CFD codes (e.g., KIVA, PHOENICS, VECTIS, FLUENT), is also considered to be valid in our analysis. This allows us to consider steady-state gas phase models, and assume that all transient processes take place in the liquid phase only. In what follows, liquid and gas phase models are considered separately.

4.1 Liquid phase models

The focus of our analysis will be on three liquid phase models:

- the model based on the assumption that there is no temperature gradient inside droplets (Infinite Thermal Conductivity (ITC) model)
- the model taking into account finite liquid thermal conductivity, but not re-circulation inside droplets (conduction limit model)
- the model taking into account both finite liquid thermal conductivity and re-circulation inside droplets via the introduction of a correction factor to the liquid thermal conductivity (Effective Thermal Conductivity (ETC) model).

These are the ones which are either used in most practical applications, including CFD codes, or which could feasibly be incorporated.

4.1.1 ITC model

For the ITC model the droplet temperature can be found from the energy balance equation (Sazhin, 2006):

$$\frac{4}{3}\pi R_d^3 \rho_l c_l \frac{\mathrm{d}T_d}{\mathrm{d}t} = 4\pi R_d^2 h (T_g - T_d), \tag{7}$$

where c_l is liquid specific heat capacity, T_g and T_d are ambient gas and droplet temperatures respectively, h is the convection heat transfer coefficient. Approximations for h depend on the processes in the gas phase, as discussed in the next subsection. Equation (7) has a straightforward analytical solution, which is widely used in most CFD codes (Sazhina et al., 2000; Wang and Rutland, 2007).

The application of this model is sometimes justified by the fact that liquid thermal conductivity is much higher than that of gas. However, the main parameter which controls droplet transient heating is not its conductivity, but its diffusivity. As mentioned earlier, in the case of Diesel engine sprays, the diffusivity for liquid is more than an order of magnitude less than that for gas. This raises the question of whether this model is applicable to modelling transient fuel droplet heating in these engines.

4.1.2 Conduction limit model

If the liquid thermal conductivity is not infinitely large then the effects of temperature gradient inside droplets need to be taken into account. As the first approximation, we can ignore effects of convection and consider the conduction limit. Assuming that droplet heating is spherically symmetric, the transient heat conduction equation inside droplets can be written as (Carslaw and Jaeger, 1986; Luikov, 1968; Kartashov, 2001):

$$\frac{\partial T}{\partial t} = \kappa_l \left(\frac{\partial^2 T}{\partial R^2} + \frac{2}{R}\frac{\partial T}{\partial R} \right) + P(R), \tag{8}$$

where $\kappa_l = k_l/(c_l \rho_l)$ is the liquid thermal diffusivity, k_l is the liquid thermal conductivity, $T = T(R,t)$ is the droplet temperature, R is the distance from the centre of the droplet and $P(R)$ is the normalised power generated per unit volume inside the droplet due to thermal radiation (in K/s). c_l, ρ_l and k_l are assumed to be constant for the analytical solution of equation (8). Their variations with temperature and time are accounted for when the analytical solution of this equation is incorporated into the numerical code.

Assuming that the droplet is heated by convection from the surrounding gas, and cooled due to evaporation, the energy balance equation at the droplet surface can be written as:

$$T_{\mathrm{eff}} - T_s = \frac{k_l}{h}\frac{\partial T}{\partial R}\bigg|_{R=R_d}, \tag{9}$$

where $T_{\mathrm{eff}} = T_g + \frac{\rho_l L \dot{R}_d}{h}$, $h = h(t)$ is the convection heat transfer coefficient (time dependent in the general case), T_s is the droplet's surface temperature, L is the specific heat of evaporation. We took into account that $\dot{R}_d < 0$. Equation (9) can be considered as a boundary condition for equation (8) at $R = R_d$. This needs to be complemented by the boundary condition at $R = 0$: $\frac{\partial T}{\partial R}|_{R=0} = 0$ and the initial condition: $T(t=0) = T_0(R)$.

The value of $\dot{R}_d$ is controlled by fuel vapour diffusion from the droplet surface. It can be found from the equation (Sazhin, 2006):

$$\dot{m}_d = 4\pi R_d^2 \dot{R}_d \rho_l = -2\pi \overline{\rho}_g D_{Fa} R_d \mathrm{Sh}_0 \ln(1 + B_M), \tag{10}$$

where $\overline{\rho}_g$ is the average gas (mixture of air and fuel vapour) density, D_{Fa} is the binary diffusion coefficient of fuel vapour in air, $\mathrm{Sh}_0 \equiv 2h_m R_d/D_{Fa}$ is the Sherwood number of non-evaporating droplets, h_m is the mass transfer coefficient. $B_M = (Y_{fs} - Y_\infty)/(1 - Y_{fs})$ is the Spalding mass transfer number, Y_{fs} and $Y_{f\infty}$ is the mass fraction of vapour near the droplet surface and at large distances from the droplet respectively. Approximations for Sh_0 depend on the modelling of the processes in the gas phase (see Subsection 4.2).

The numerical solution of equation (8) with appropriate boundary and initial conditions has been widely used for the analysis of the thermal balance of individual droplets (Wong et al., 1997; Yang and Wong, 2003; Cuoci et al., 2005; Stauch et al., 2006). To the best of our knowledge the only application of this solution in CFD codes has been reported by Bertoli and na Migliaccio (1999). In all these papers, the effects of thermal radiation were ignored altogether or taken into account via the modification of the boundary conditions, as by Cuoci et al. (2005). The latter is justified only in the case of strongly absorbent droplets, which are a poor approximation in the case of Diesel fuel droplets (Dombrovsky et al., 2001; Sazhin et al., 2004a, 2007b).

An alternative approach to implementation of the finite liquid thermal conductivity model into CFD codes is based on the analytical solution of equation (8) with appropriate boundary and initial conditions. In the case when $h(t) = h = \mathrm{const}$, this solution can be presented as (Sazhin et al., 2004b):

$$T(R,t) = \frac{R_d}{R}\sum_{n=1}^{\infty}\left\{\frac{p_n}{\kappa\lambda_n^2} + \exp\left[-\kappa\lambda_n^2 t\right]\left(q_n - \frac{p_n}{\kappa\lambda_n^2}\right) - \frac{\sin\lambda_n}{\|v_n\|^2\lambda_n^2}\mu_0(0)\exp\left[-\kappa\lambda_n^2 t\right] - \frac{\sin\lambda_n}{\|v_n\|^2\lambda_n^2} \times \int_0^t \frac{\mathrm{d}\mu_0(\tau)}{\mathrm{d}\tau}\exp\left[-\kappa\lambda_n^2(t-\tau)\right]\mathrm{d}\tau\right\} \times \sin(\lambda_n R/R_d) + T_{\mathrm{eff}}(t), \quad (11)$$

where:

$$\mu_0(t) = \frac{hT_{\mathrm{eff}}(t)R_d}{k_l}, \quad h_0 = (hR_d/k_l) - 1,$$

$$\|v_n\|^2 = \frac{1}{2}\left(1 + \frac{h_0}{h_0^2 + \lambda_n^2}\right),$$

$$\kappa = \frac{k_l}{c_l\rho_l R_d^2},$$

$$p_n = \frac{1}{R_d\|v_n\|^2}\int_0^{R_d}\widetilde{P}(R)v_n(R)\mathrm{d}R,$$

$$q_n = \frac{1}{R_d\|v_n\|^2}\int_0^{R_d}\widetilde{T}_0(R)v_n(R)\mathrm{d}R,$$

$$\widetilde{P}(R) = RP(R)/(c_l\rho_l R_d), \quad \widetilde{T}_0(R) = RT_0(R)/R_d,$$

$$v_n(R) = \sin(\lambda_n R/R_d) \quad (n = 1, 2, \ldots),$$

a set of positive eigenvalues λ_n numbered in ascending order ($n = 1, 2, \ldots$) is found from the solution of the following equation:

$$\lambda\cos\lambda + h_0\sin\lambda = 0.$$

If $T_0(R)$ is twice differentiable, then the series in equation (11) converges absolutely and uniformly for all $t \geq 0$ and $R \in [0, R_d]$. The details of the implementation of Solution (11) into a zero-dimensional CFD code are discussed by Sazhin et al. (2005a, 2005b).

4.1.3 Effects of thermal radiation

It was shown that using a realistic model for $P(R)$, taking into account the actual dependence of P on R, leads to a very small improvement in the accuracy of the prediction when compared with the simplified model in which only the integral absorption of thermal radiation in the droplet is taken into account (Abramzon and Sazhin, 2005, 2006). In the latter model $P(R)$ is approximated as (Dombrovsky et al., 2001; Sazhin et al., 2004a, 2007b):

$$P(R) = 3 \times 10^6 a\sigma R_{d(\mu\mathrm{m})}^{b-1}\theta_R^4/(c_l\rho_l), \quad (12)$$

where θ_R is the radiation temperature, $R_{d(\mu\mathrm{m})}$ is the droplet radius in μm, a and b are polynomials of the radiation temperature (quadratic functions in the first approximation). The effects of radiation are expected to be significant during the late injection of spray when the flame has already developed (Sazhin et al., 2006). In our case, however, the focus is on the modelling of the autoignition process, when these effects can be safely ignored.

4.1.4 ETC model

The conduction limit model can be generalised to take into account the internal re-circulation inside droplets. This can be achieved by replacing the thermal conductivity of liquid k_l with the so called Effective Thermal Conductivity (ETC) $k_{\mathrm{eff}} = \chi k_l$, where the coefficient χ varies from about 1 (at droplet Peclet number $\mathrm{Pe}_d = \mathrm{Re}_{ld}\mathrm{Pr}_{ld} < 10$) to 2.72 (at $\mathrm{Pe}_d > 500$). It can be approximated as (Abramzon and Sirignano, 1989):

$$\chi = 1.86 + 0.86\tanh[2.225\log_{10}(\mathrm{Pe}_d/30)].$$

The values of transport coefficients in Pe_d are taken for liquid fuel. The relative velocity of droplets and their diameters are used for calculation of Re_{ld}. This model, known as the ETC model, has been implemented into the customised version of the KIVA 2 code alongside the analytical solution (11). Additional complications are expected in the case of heating and evaporation of multicomponent droplets (see e.g., Arias-Zugasti and Rosner, 2003), but the analysis of this case is beyond the scope of this paper.

The practical application of the models described above depends on the choice of the approximations for Sh_0 and Nu. These will follow from the analysis of gas phase models discussed in the next subsection.

4.2 Gas phase models

Various gas phase models suitable for implementation into CFD codes have been analysed in a number of papers including those by Miller et al. (1998) and Sazhin et al. (2006). The simplest model of droplet heating and evaporation in which the effect of superheat of fuel vapour is taken into account leads to the following approximations for Sh_0 and Nu (Lefebvre, 1989; Bird et al., 2002):

$$\mathrm{Sh}_0 = 2\big(1 + 0.3\mathrm{Re}_d^{1/2}\mathrm{Sc}_d^{1/3}\big), \tag{13}$$

$$\mathrm{Nu} = 2\frac{\ln(1+B_M)}{B_M}\big(1 + 0.3\mathrm{Re}_d^{1/2}\mathrm{Pr}_d^{1/3}\big), \tag{14}$$

where $\mathrm{Re}_d = 2R_d|\mathbf{v}_d - \mathbf{v}_g|/\bar{\nu}_g$, $\mathrm{Sc}_d = \bar{\nu}_g/D_{Fa}$ and $\mathrm{Pr}_d = \bar{c}_{pg}\bar{\mu}_g/\bar{k}_g$ are Reynolds, Schmidt and Prandtl numbers of the moving droplets respectively, $\mathbf{v}_d$ and $\mathbf{v}_g$ are droplet and gas velocities respectively, $\bar{\nu}_g$ and $\bar{\mu}_g$ are average gas kinematic and dynamic viscosities, $\bar{c}_{pg}$ and $\bar{k}_g$ are average gas specific heat capacity at constant pressure and thermal conductivity; the temperature dependence of all parameters is taken into account. In what follows this model will be referred to as Model 0.

As follows from the analysis of various gas phase models, presented by Sazhin et al. (2006), the model described by equations (13)–(14) is one of the least accurate ones. In the same paper it was shown that the most accurate model is the one suggested by Abramzon and Sirignano (1989). In this model Sh_0 and Nu are given by the following expressions:

$$\mathrm{Sh}_0 = 2\left(1 + \frac{(1+\mathrm{Re}_d\mathrm{Sc}_d)^{1/3}\max[1,\mathrm{Re}_d^{0.077}] - 1}{2F(B_M)}\right), \tag{15}$$

$$\mathrm{Nu} = 2\frac{\ln(1+B_T)}{B_T} \times \left(1 + \frac{(1+\mathrm{Re}_d\mathrm{Pr}_d)^{1/3}\max[1,\mathrm{Re}_d^{0.077}] - 1}{2F(B_T)}\right), \tag{16}$$

where

$$F(B_{M,T}) = (1+B_{M,T})^{0.7}\frac{\ln(1+B_{M,T})}{B_{M,T}},$$

$$B_T = \frac{c_{pF}(T_g - T_s)}{L_{\mathrm{eff}}}$$

(Spalding heat transfer number), $L_{\mathrm{eff}} = L + \frac{Q_L}{\dot{m}_d}$, Q_L is the power spent on droplet heating, c_{pF} is the specific heat capacity of fuel vapour. B_T can be calculated based on the following relation:

$$B_T = (1+B_M)^{\varphi} - 1, \tag{17}$$

where

$$\varphi = \frac{1 + \frac{(1+\mathrm{Re}_d\mathrm{Sc}_d)^{1/3}\max[1,\mathrm{Re}_d^{0.077}]-1}{2F(B_M)}}{1 + \frac{(1+\mathrm{Re}_d\mathrm{Pr}_d)^{1/3}\max[1,\mathrm{Re}_d^{0.077}]-1}{2F(B_T)}}\left(\frac{c_{pF}}{\bar{c}_{pg}}\right)\frac{1}{\mathrm{Le}}, \tag{18}$$

$\mathrm{Le} = k_g/(\bar{c}_{pg}\bar{\rho}_g D_{Fa})$ is the Lewis number. In what follows this model will be referred to as the Abramzon and Sirignano (AS) Model.

Both these models have been implemented into the customised version of the KIVA 2 code to investigate the effect of gas phase models on the performance of this code.

The effect of gas turbulence was accounted for based on the conventional $k-\epsilon$ model implemented in the KIVA 2 code (see Demoulin and Borghi (2003) and Wright et al. (2005) for more advanced approaches to turbulence modelling).

5 Shell autoignition model

The most rigorous approach to modelling the autoignition process in Diesel engines is based on the Detailed Kinetic Mechanism (DKM), which includes about 1000 chemical reactions and over 100 species (Minetti et al., 1994; Kojima, 1994; Ranzi et al., 1994; Cuoci et al., 2005). Additional problems in the construction of DKMs arise from the lack of accurate kinetic data for many of the reactions. Even quantum chemistry methods cannot ensure accurate calculation of rate constants because the decisive factor in this calculation is the small value difference between the high energy levels of reacting molecules (Basevich, 1990). These factors prove to be very restrictive for the application of DKM in engineering CFD codes.

A number of reduced chemical models have been suggested (e.g., Müller et al., 1992; Basevich and Frolov, 1994; Griffiths, 1995; Porter et al., 2007). The model which is used in our study is widely known as the Shell model (Halstead et al., 1977). In this model the autoignition chemistry is reduced to the eight-step chain branching reaction scheme and incorporated into four processes:

Initiation:

$\mathrm{RH} + \mathrm{O}_2 \rightarrow 2\mathrm{R}^*$ Rate coefficient k_q

Propagation:

$\mathrm{R}^* \rightarrow \mathrm{R}^* + \mathrm{P}$ Rate coefficient k_p

$\mathrm{R}^* \rightarrow \mathrm{R}^* + \mathrm{B}$ Rate coefficient $f_1 k_p$

$\mathrm{R}^* \rightarrow \mathrm{R}^* + \mathrm{Q}$ Rate coefficient $f_4 k_p$

$\mathrm{R}^* + \mathrm{Q} \rightarrow \mathrm{R}^* + \mathrm{B}$ Rate coefficient $f_2 k_p$

Branching :

$\mathrm{B} \rightarrow 2\mathrm{R}^*$ Rate coefficient k_b

Termination :

$\mathrm{R}^* \rightarrow \mathrm{out}$ Rate coefficient $f_3 k_p$

$2\mathrm{R}^* \rightarrow \mathrm{out}$ Rate coefficient k_t

RH represents hydrocarbon fuel ($\mathrm{C_nH_{2m}}$), R^* the radical, B the branching agent, Q the intermediate agent, and P is the product, consisting of CO, $\mathrm{CO_2}$ and $\mathrm{H_2O}$. Further development of this model has been discussed by a number of authors (see Sazhin et al., 1999; Hamosfakidis and Reitz, 2003; Ribaucour et al., 2007 and the references therein). Possible adaptation of the Shell model to modelling the

autoignition process in Diesel engines was discussed by Sazhina et al. (1999, 2000). It was suggested that the original version of the Shell model could be adapted to Diesel engine environments via the modification of just one constant, A_{f4}, in the equation for the intermediate agent:

$$\frac{\mathrm{d[Q]}}{\mathrm{d}t} = f_4 k_p[\mathrm{R}^*] - f_2 k_p[\mathrm{Q}][\mathrm{R}^*], \tag{19}$$

where

$$f_2 = A_{f2}\exp(-E_{f2}/R_u T),$$
$$f_4 = A_{f4}\exp(-E_{f4}/R_u T), [O_2]^{x4}[RH]^{y4}$$
$$k_p = \left[\frac{1}{k_{p1}[O_2]} + \frac{1}{k_{p2}} + \frac{1}{k_{p3}[RH]}\right]^{-1},$$

R_u is the universal gas constant, [M] corresponds to the molar concentration of the various species M. The values of constants in these expressions for various fuels are given by Halstead et al. (1977). It was recommended that the Shell model should be used for modelling autoignition in Diesel engines if all its coefficients, except A_{f4}, are taken equal to those found by Halstead et al. (1977) for the primary reference fuel RON70, and A_{f4} is taken in the range 3×10^6 to 6×10^6 (Sazhina et al., 1999, 2000). This model has been implemented into the KIVA 2 code and is used in our analysis.

6 Experimental set-up

High-speed Diesel sprays have been studied experimentally at the University of Brighton using various optical diagnostic techniques (Crua, 2002). These studies were conducted in a rapid compression machine based on a single cylinder Ricardo Proteus test engine which was converted to a two-stroke cycle. The engine had a bore of 135 mm, a stroke of 150 mm and a displacement of 2.2 litres. The Proteus rig was coupled to a DC dynamometer via reduction belts. An optical chamber, 80 mm in length and 50 mm in diameter, was fitted on the cylinder head to investigate the spray development. This allowed a fuel spray to be injected vertically without any impingement on the walls or the windows. A second generation Bosch common rail fuel injection system was used to generate the high pressure required to maintain injection pressure ranging from 60 MPa to 160 MPa. The fuel pump was driven externally via an electrical motor running at 1400 rpm to maintain the required high pressure in the fuel rail with minimum fluctuation (Crua, 2002). The main parameters which were studied using this set-up were spray penetration and autoignition delay.

Spray penetration was studied using Kodak Ektapro HS Motion Analyser, with a recording rate adjustable up to 4500 frames per second at maximum resolution. The processing of the video images for measurement of the spray penetration was performed by purpose-developed software. From analysis of the luminosity of the spray video images, information about the length of the visible part of the spray was obtained. This length, defined as spray penetration, was assumed to be equal to the distance from the nozzle to the furthest point on the spray axis where the luminosity was above a given threshold. It was assumed that the spray luminosity varies smoothly along the spray, and the effect of cluster shedding from the spray tip was ignored. The rate of injection was measured as a function of time using a Lucas rate tube.

Ignition delay is defined as the total autoignition delay after the start of injection. It consists of physical and chemical delays. In experiments, the total delay has been measured using two different methods. The first method is based on the assessment of the flame luminosity from spray video records which capture the ignition spark. The second method is based on the analysis of the pressure traces. Typically, the first method captures the earliest stage of autoignition, while the second one gives a strong indication of the start of combustion. The errors of each of these two methods do not exceed about 20%, for the range of conditions studied (Crua, 2002). Both methods were used simultaneously in order to assess their complementary nature (Crua, 2002). In our study the timing of the autoignition is identified based on the flame luminosity.

In order to record the autoignition processes, two high-speed CCD video cameras were placed at 90° to each other. The cameras have resolution 128×64 pixels $\times$ 256 grey levels, with a sensitivity equivalent to 3000 ISO and recording speed up to 27,000 frames per second. Both cameras were triggered by the same dedicated signal emitted by the custom-built FIE controller. In order to further maximise the sensitivity of the recordings, the lens was set to its widest aperture ($f/1.9$). The time at which the first portion of liquid fuel was seen leaving the nozzle was measured to be 0.37 ms after the start of recording for an injection pressure of 160 MPa. The data were adjusted to compensate for this delay.

7 Test cases

The test cases chosen for the analysis were based on the measurements of sprays under realistic conditions of operation for a light-duty Diesel engine with a single-hole injector of 0.2 mm in diameter, located on the axis at the top centre of a cylindrical combustion chamber. The fuel injection pressure was 160 MPa, the monitored in-cylinder pressures at Top Dead Centre (TDC) were 5.6, 6.2, and 6.9 MPa. At the start of injection, the gas pressure was assumed to be equal to experimentally measured pressure at TDC, while the temperature was estimated based on the intake gas pressure and temperature, and the air compression ratio. The polytropic law was used with the polytropic coefficient calculated based on the plots $\log p$ vs. $\log V$ for each individual pressure at TDC (Lacoste, 2005). The comparison was performed for initial gas pressures in the approximate range 2.5–8.5 MPa. The values of temperature for various pressures, obtained using this method are indicated as filled circles in Figure 4. The solid lines on the same figure were used for the estimate

of temperature at other pressures, including those in the test cases. The temperature values calculated using this procedure are shown in Table 1. It was assumed that the chamber was filled with dry air (71% nitrogen and 29% oxygen by volume). The errors of calculation were estimated to be ± 50 K. The values of autoignition delay time, defined as the time from the start of injection to the first appearance of a visible flame on the video recordings (Crua, 2002), are presented in Table 1.

Figure 4 The initial in-cylinder gas temperatures at the Top Dead Centre (TDC) as a function of the initial gas pressure at TDC. Filled circles refer to the values of this temperature, calculated from the polytropic law

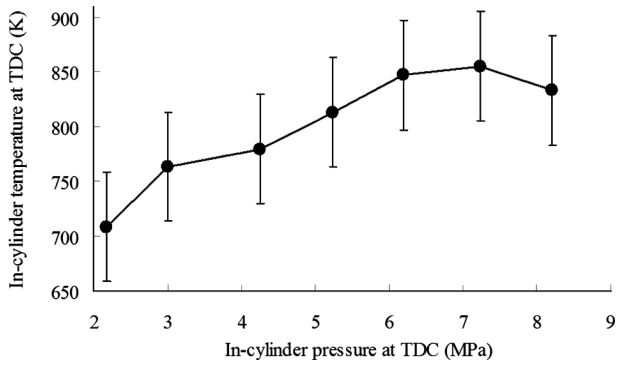

Table 1 The values of the measured autoignition delay times (ADT) and calculated initial in-cylinder gas temperatures (T) for various in-cylinder pressures (P)

P (MPa)	*T* (K)	*ADT* (ms)
5.6	832	2.37
6.2	847	2.04
6.9	852	1.78

8 Results

For the chosen test cases computations were performed assuming axial symmetry of the flow. Variations in the volume of the combustion chamber caused by piston motion during the injection pulse were small and, therefore, were ignored in the computations. As in the case considered in Section 3, the domain was covered by a uniform 2-dimensional grid, typically with 20 cells in the radial and 48 cells in the axial directions. In computations, the liquid spray penetration is defined as the distance from the nozzle to the leading droplet parcel in the spray. The ignition delay is defined as the moment after the start of injection when the local gas temperature rises above the critical threshold of 1100 K (Sazhina et al., 2000). Injection velocities were calculated from the measured rate of injection (Karimi et al., 2006) (see Figure 1).

The fuel injector could be heated up to 350–400 K. In most cases the temperature of the droplet parcels emerging from the injector was set to 375 K. A special study was undertaken to determine the sensitivity of the results to variations in the liquid fuel temperature.

The following analysis is sub-divided into two parts. The analysis of autoignition delay characteristics is presented in Section 8.1. The analysis of pre-ignition spray characteristics is presented in Section 8.2.

8.1 Autoignition delay

At first the modified WAVE breakup model was used and the parameter A_{f4} in the Shell model was assumed equal to 3×10^6. The predictions of the KIVA 2 code with two liquid phase models (ITC and ETC) and two gas phase models (Model 0 and the Abramzon and Sirignano (AS) Model) were compared with experimental data. The results are shown in Figure 5. As follows from this figure, the choice of the liquid phase model has a much stronger effect on the autoignition delay compared with the gas phase model. This agrees with the previously reported results based on a zero-dimensional code (Sazhin et al., 2006). This provides additional support for the recommendation made by Sazhin et al. (2006) that the more accurate ETC model, rather than the ITC model, should be used for the reliable prediction of autoignition delay. All models predict correctly the decrease in autoignition delay with increasing in-cylinder pressure. However, there is a noticeable (up to about 10%) deviation between experimental data and the predictions of all models, especially at relatively low pressures. This can be attributed to uncertainty about the choice of other parameters used in the modelling as discussed later in this section. A similar decrease in ignition delay with increasing in-cylinder pressure was observed for injection pressure 100 MPa. However, we could not compare the results for this injection pressure with the prediction of the model as measurements of the fuel injection rate were not performed for this case. At higher in-cylinder gas pressures (more than about 7 MPa for 160 MPa injection pressure, and 8 MPa for 100 MPa injection pressure), the measurements show an increase in ignition delay time with gas pressure (Crua, 2002; Crua et al., 2004). However, this trend is not reproduced by the model. This can be attributed to the limitations of the ideal-gas approximations for the fuel-air mixture at high in-cylinder pressures. Possible other explanations of this trend are discussed by Crua et al. (2004). Note that error bars referring to experimental data are not symmetric.

Figure 6 shows the effect of breakup models on the autoignition delay in Diesel sprays. The ETC liquid phase model and the AS gas phase model were used for calculations. As can be seen from this figure, the variations in the autoignition delay time caused by the choice of the breakup model are less than about 2.5%, which is within accuracy of the experimental data. Strong jet accelerations during the first 0.2 ms after the injection, which affect the spray breakup at the initial stage of injection (during about 1 ms), have little effect on spray properties at the time of autoignition (about 2 ms after injection). This explains the relatively small difference between the autoignition delays calculated using the conventional and modified WAVE breakup models. The fact that the TAB breakup model predicts slightly shorter ignition delays than the

WAVE models can be explained by the fact that the TAB model predicts the generation of larger amounts of smaller droplets which evaporate quickly (cf., Figure 3).

Figure 5 The total autoignition delay times observed experimentally and computed using the customised version of the KIVA 2 CFD code at three initial in-cylinder pressures. The values of the initial gas temperature were obtained from Figure 4. The initial injected liquid fuel temperature was assumed equal to 375 K. The injection pressure was equal to 160 MPa. The modified WAVE model, two liquid phase models (ETC and ITC) and two gas phase models (model 0 and the AS model) were used for computations

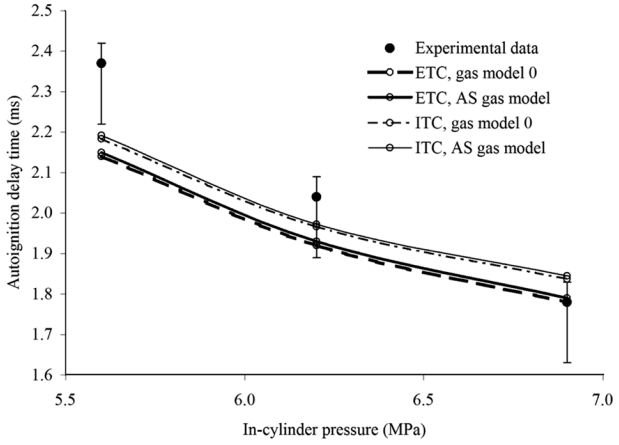

Figure 6 The same as Figure 5, but the computations were based on the ETC liquid phase model, the AS gas phase model and various droplet breakup models (the same as in Figures 2 and 3)

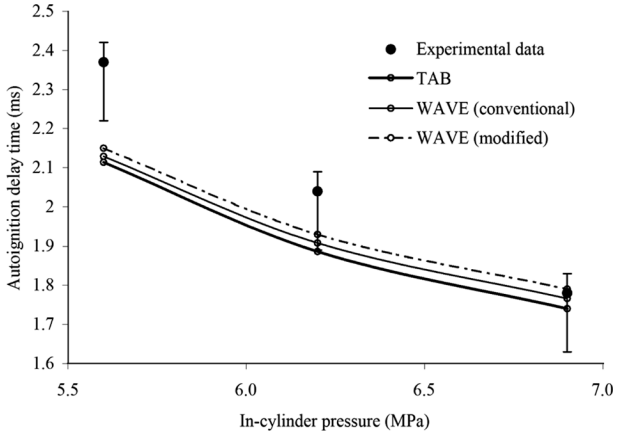

As follows from Figure 4, there is uncertainty about the estimation of the initial gas temperature in the combustion chamber, variations of ± 50 K are expected. The sensitivity analysis of the results with respect to the choice of the initial gas temperature are shown in Figure 7. The ETC liquid phase model, the AS gas phase model and the modified WAVE model were used for calculations. The results of computations, based on the initial gas temperatures estimated from the measurements (reference temperature), as shown in Table 1, are represented by the solid curve. Thin and thick dashed curves show the ignition delays predicted based on the assumption that the initial gas temperature is 20 K higher and 20 K lower than the reference temperature respectively. As follows from Figure 7, the effect of the initial gas temperature on the predicted autoignition delay is rather strong (up to about 20%). The autoignition delay decreases with increasing gas temperature, as expected. The best agreement with experimental data was achieved when we used the initial gas temperature 20 K below the reference one.

Figure 7 The same as Figsure 5 and 6, but the computations were based on the ETC liquid phase model, the AS gas phase model, the modified WAVE model and three values of the initial gas temperature. Firstly, the initial gas temperatures was taken equal to the one predicted by Figure 4; secondly, this temperature was taken equal to the one predicted by this figure minus 20 K; thirdly, this temperature was taken equal to the one predicted by this figure plus 20 K

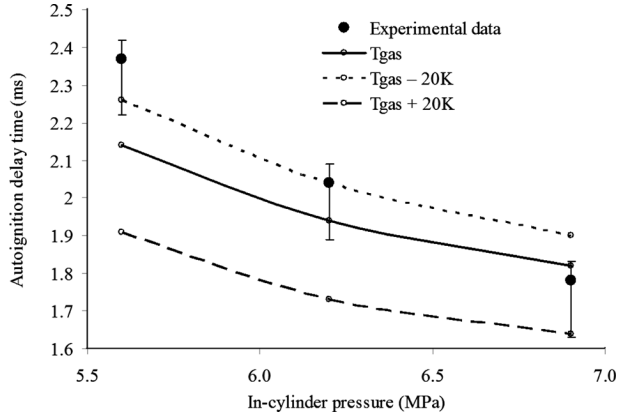

Figure 8 shows the effect of the temperature of injected fuel on the autoignition delay. As in the case of Figure 7, the ETC liquid phase model, the AS gas phase model and the modified WAVE model were used for calculations. The initial gas temperatures were taken from Table 1. As follows from Figure 8, the decrease in the injection fuel temperature from 375 K to 350 K leads to a very small increase in the autoignition delay. However, the increase in this temperature from 375 K to 400 K leads to quite a significant decrease in this delay, especially for in-cylinder pressure of 6.2 MPa. Since this increase in the injected fuel pressure leads to considerable deviation between the experimental and computed results, it seems unlikely that the value of this temperature will reach 400 K.

As was shown by Sazhina et al. (2000), the increase of parameter A_{f4} leads to a decrease in the chemical autoignition delay time. At the next stage of our analysis the sensitivity of the predicted ignition delay to the values of A_{f4} was investigated. The results for the same models and values of parameters as in Figures 5–8, but for various A_{f4} are shown in Figure 9. Following Sazhina et al. (1999, 2000), the analysis was focused on A_{f4} in the range 3×10^6 to 6×10^6 (see Section 5). As follows from this figure, the values of the autoignition delay decrease with increasing A_{f4}, in agreement with Sazhina et al. (2000). This decrease could be up to about 20% which indicates a non-negligible role of the chemical autoignition

delay compared with the total autoignition delay in this particular case. In fact, the parameter A_{f4} could be the fitting parameter of the model if we are able to specify accurately both the initial gas temperature and injection fuel temperature.

Figure 8 The same as Figure 7, but the computations were based on three injected fuel temperatures: 350 K, 375 K and 400 K

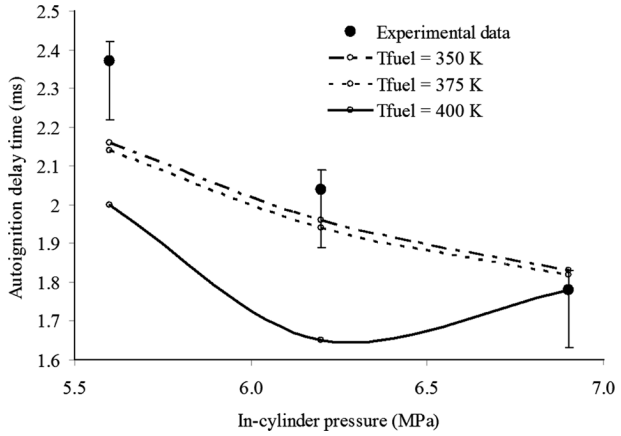

Figure 9 The same as Figure 8 for the injected fuel temperature 375 K, but the computations were based on four values of the coefficient A_{f4} in the Shell model as indicated in the figure

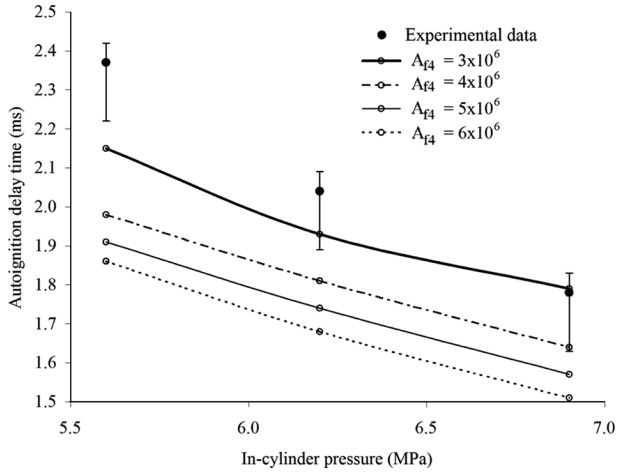

Finally, the grid sensitivity of the results shown in Figures 5–9 was investigated. The results are shown in Figure 10. The same models as in Figures 5–9 were used with injection temperature equal to 375 K and $A_{f4} = 3 \times 10^6$. As follows from this figure, the difference between the delay times predicted by computations based on various grids does not exceed about 3%. This is well below the experimental error of the results and allows us to conclude that mesh resolution, used in our computations, is sufficient to achieve accurate results.

8.2 Pre-ignition spray characteristics

In this subsection a number of spray characteristics, mainly at the pre-ignition stage, are discussed. No direct experimental verification of the results will be available in most cases, but these results are expected to allow us to develop a better understanding of the processes which cannot be directly observed at the moment.

Figure 11 shows the time dependence of the Sauter Mean Radius (SMR) of droplets and maximal in-cylinder pressure predicted by the KIVA 2 code with the modified WAVE model, the ETC liquid phase model and the AS gas phase model. The injection pressure was taken equal to 160 MPa, the initial gas pressure was equal to 6.2 MPa, the fuel injection temperature was taken equal to 375 K. The same grid as in Section 8.1 was used. As follows from Figure 11, the SMR of droplets rapidly reduces to about 10 μm, due to the breakup processes. This value of the SMR is of the same order of magnitude as observed experimentally (cf. Figure 3). The initial small peak of the maximal in-cylinder pressure is related to the compression of air during the injection process.

Figure 10 The same as Figure 9, but for $A_{f4} = 3 \times 10^6$, the computations were based on four grid arrangements as indicated in the figure

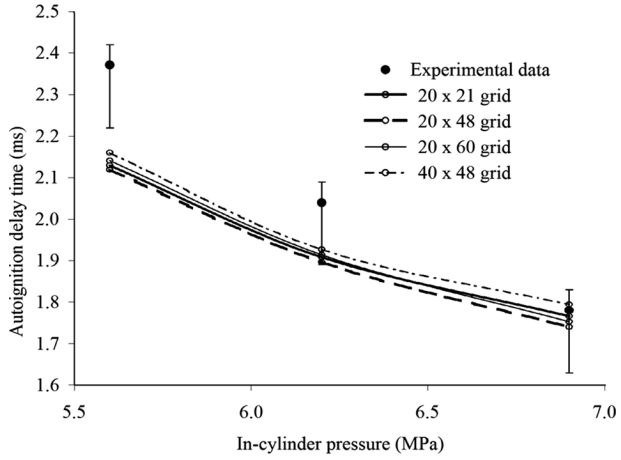

Figure 11 The time evolution of the maximal Sauter Mean Radii (SMR) of droplets and in-cylinder gas pressure in the combustion chamber for the initial gas pressure 6.2 MPa and initial gas temperature 850 K. The modified WAVE model, the ETC liquid phase model and the AS gas phase model were used for computations

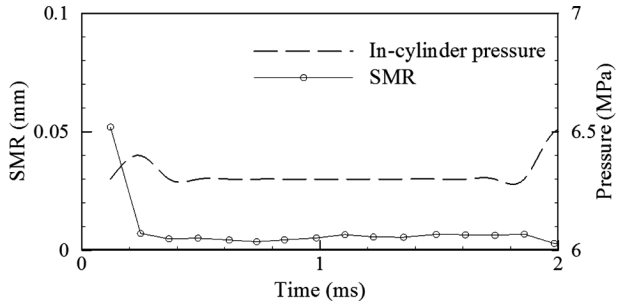

Figure 12 shows the time dependence of the maximal and minimal gas temperatures in the combustion chamber and the maximal temperature at the surface of the droplets for the same models and initial values of parameters as in Figure 11. The autoignition process at times greater

than about 1.8 ms, accompanied by a rapid increase in the maximal gas temperature, is clearly seen in this figure. The predicted initial decrease in the minimal gas temperature is clearly linked with the evaporation of freshly injected droplets. At times greater than about 0.5 ms, heat supplied by the chemical reactions seems to exceed the heat consumed for the evaporation process, and the minimal gas temperature slowly starts to increase. The increase in the maximal droplet surface temperature during about the first 0.3 ms after injection corresponds to the droplet heat-up period. After that, this temperature remains at a nearly constant level, close to the critical temperature of Diesel fuel (but always below it).

Figure 12 The same as Figure 11, but for maximal and minimal gas temperatures and maximal droplet surface temperature

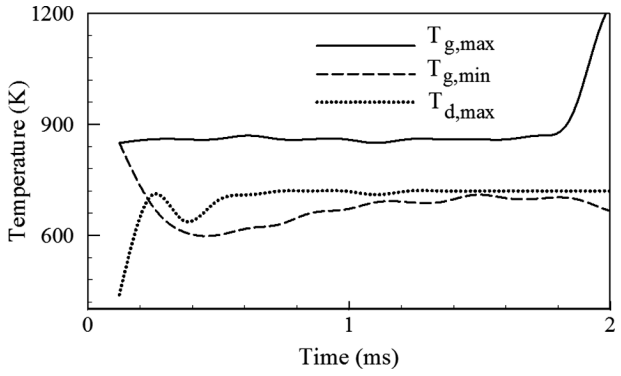

Figure 13 shows the time dependence of the maximal mass fractions of fuel vapour and the species described by the Shell model (the radicals (R), branching agent (B), and intermediate agent (Q)), and the minimal mass fraction of oxygen for the same models and initial values of parameters as in Figures 11–12. The initial increase in the fuel vapour mass fraction is related to the evaporation of liquid Diesel fuel. The autoignition stage is preceded by a slow decrease in fuel vapour and oxygen mass fractions. This is accompanied by the corresponding increase in mass fractions of radicals, branching and intermediate agents. Immediately before the onset of autoignition (sometimes about 1.8 ms), the increase in mass fractions of radicals, branching and intermediate agents is visibly accelerated. This is accompanied by a rapid decrease in the mass fraction of oxygen, while the maximal concentration of fuel vapour remains practically unchanged.

Figure 14 shows the spatial distribution of droplets in the spray at four different times after the start of injection. These moments correspond to three stages in the spray evolution: (a) breakup and heating of the liquid droplets, (b) and (c) breakup, heating, and evaporation of droplets, (d) the ignition. The same models and initial values of parameters as in Figures 11–13 were used for computations. The circles on this figure show radii of droplet parcels magnified 500 times. At the injector, the radii of droplets were specified based on the radius of the injector, taking into account the effects of flow cavitation in the nozzle: $R_{d0} = R_{\mathrm{nozzle}} \cdot C_{\mathrm{contr}}$, where $C_{\mathrm{contr}} = 0.62$ if the cavitation number CN is greater than or equal to 1, and $C_{\mathrm{contr}} = 1$ if this number is less than 1 (Sarre et al., 1999). Then the droplet radii rapidly decrease due to breakup processes. At the moment of time 0.98 ms no droplets are observed beyond Z equal to about 4.5 cm. This is due to the limitation of the penetration length at this moment. At $t = 1.49$ ms the droplets are observed over the whole range of Z. At $t = 1.73$ ms the number of droplets beyond $Z = 4.5$ cm is visibly reduced, alongside their SMR. This is related to droplet evaporation processes. These reductions were clearly visible at $t = 1.98$, where autoignition took place and the increased gas temperature led to even more rapid droplet evaporation.

Figure 13 The same as Figures 11–12, but for the maximal mass fractions of fuel vapour and the species described by the Shell model (the radicals (R), branching agent (B), and intermediate agent (Q)), and the minimal mass fraction of oxygen

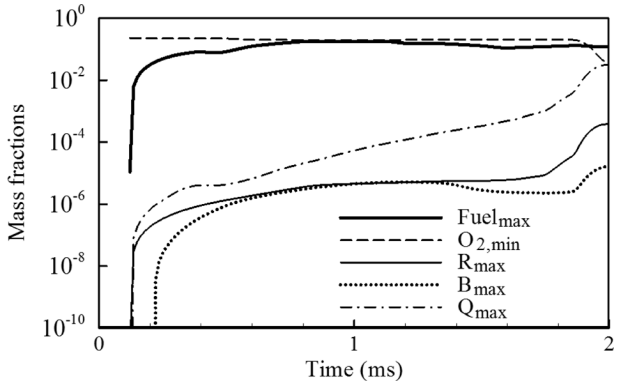

Figure 14 Spatial distribution of droplets at four moments of time for the same values of the initial parameters and models as in Figure 11. The circles show SMR of droplets magnified 500 times

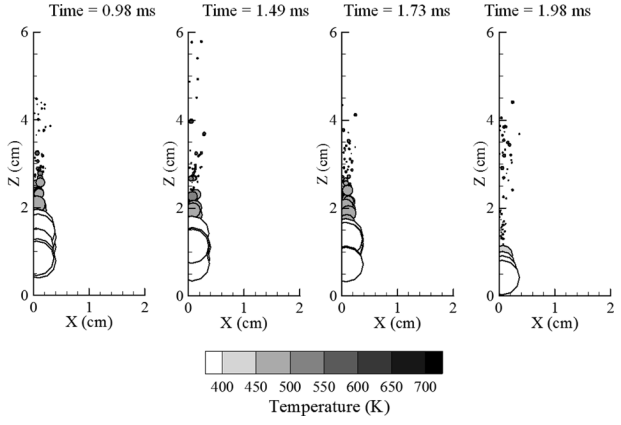

The spatial distribution of gas temperatures, SMR, mass fractions of fuel vapour, oxygen, branching agent, radicals and intermediate agent for the same moments of time as in Figure 14 are shown in Figures 15–17. The same models and initial values of parameters as in Figures 11–14 were used for computations. As follows from Figure 15, before autoignition the slow increase in gas temperature takes place in the area away from

the spray. In the immediate vicinity of the spray, gas is cooled due to the evaporation process. After autoignition, a rapid increase in gas temperature takes place mainly at the periphery of the spray, in agreement with the early results reported by Flynn et al. (1999) and Sazhina et al. (2000). The distribution of the SMR shown in Figure 15 is generally consistent with the distribution of droplets shown in Figure 14.

Figure 15 Spatial distributions of gas temperature and SMR of droplets for the same moments of time, values of the initial parameters and models as in Figure 14

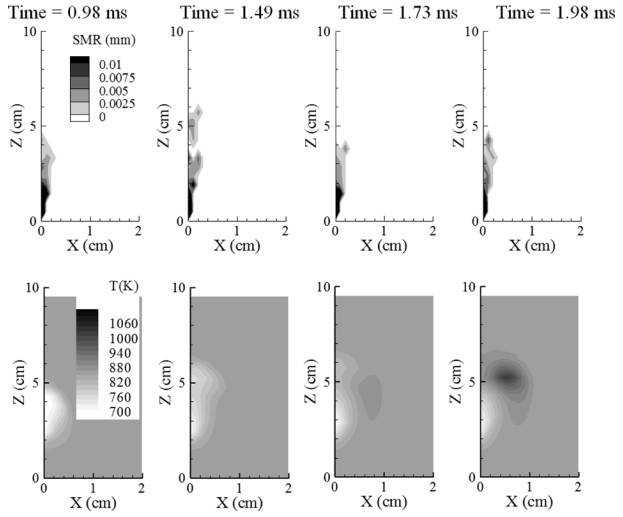

Figure 16 The same as Figure 15, but for the fuel vapour and oxygen relative mass fractions

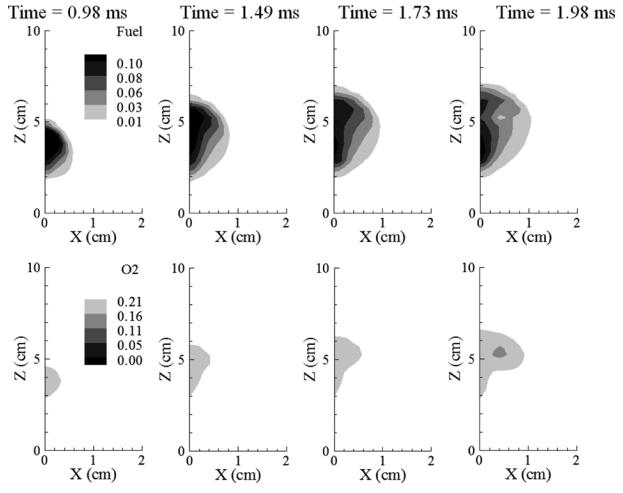

As follows from Figure 16, for t between 0.98 ms and 1.73 ms, the fuel vapour mass fraction gradually increases and this vapour spreads from the vicinity of the spray to the ambient gas, while the maximal fuel vapour mass fraction remains practically unchanged (see Figure 13). At $t = 1.98$ ms a visible decrease in fuel vapour mass fraction can be seen at the spray periphery where the autoignition took place. The decrease in oxygen mass fraction at the same time and at the same location can be clearly seen in the same Figure 16. Visible increases in mass fractions of the branching agent, radicals and intermediate agent at $t = 1.98$ ms, near the periphery of the spray, can be clearly seen in Figure 17.

Figure 18 shows the evolution of droplet parameters in various ranges of droplet radii at the same moments of time as in Figures 14–17. Eight bands were considered, as shown in Table 2:

Table 2 Bands of droplet radii

Band	*Range*
1	$R_d \leq 1.32$ μm
2	$1.32 < R_d \leq 4.44$ μm
3	$4.44 < R_d \leq 10.5$ μm
4	$10.5 < R_d \leq 20.6$ μm
5	$20.6 < R_d \leq 35.6$ μm
6	$35.6 < R_d \leq 56.5$ μm
7	$56.5 < R_d \leq 82.0$ μm
8	$R_d > 82.0$ μm

In Figure 18 bands 1–5 are shown, as these are the most representative for the presentation of the evolution of spray parameters. Droplets with radii greater than about 35 μm (bands 6–8) disappear from the system due to the breakup processes.

As follows from this figure, at $t = 0.98$ ms, the droplets with radii up to about 30 μm are present in the system. By $t = 1.98$ ms, the droplets with radii greater than about 20 μm practically disappear from the system due to the breakup and evaporation processes. At all stages the surface temperatures of larger droplets are lower than those of smaller droplets. This is explained by the fact that large, fresh droplets are continuously injected into the system and that they require more time to heat-up compared with smaller ones. The relative speeds of larger droplets are always higher than those of smaller ones, as smaller droplets are more easily entrained by the ambient air than larger ones.

9 Conclusions

A number of new models have been implemented into the customised version of the KIVA 2 CFD code. These are the modified WAVE droplet breakup model, taking into account transient processes during spray injection, the ETC liquid phase model, the gas phase model suggested by Abramzon and Sirignano (1989), and the customised version of the Shell autoignition model. The predictions of the updated KIVA 2 code have been compared with the results of the in-house experimental studies of Diesel sprays where appropriate. The measurable spray parameters include spray penetration length, the time evolution of the Sauter Mean Radius (SMR) of droplets and autoignition delay times. Both spray injection into a relatively 'cold' gas, not leading to the autoignition process, and into a 'hot' gas, leading to this process, have been considered.

It has been pointed out that in the case of spray injection into 'cold' gas, the observed spray tip penetration agrees much better with the prediction of the modified

Figure 17 The same as Figures 15 and 16, but for the branching agent, radicals and intermediate agent relative mass fractions

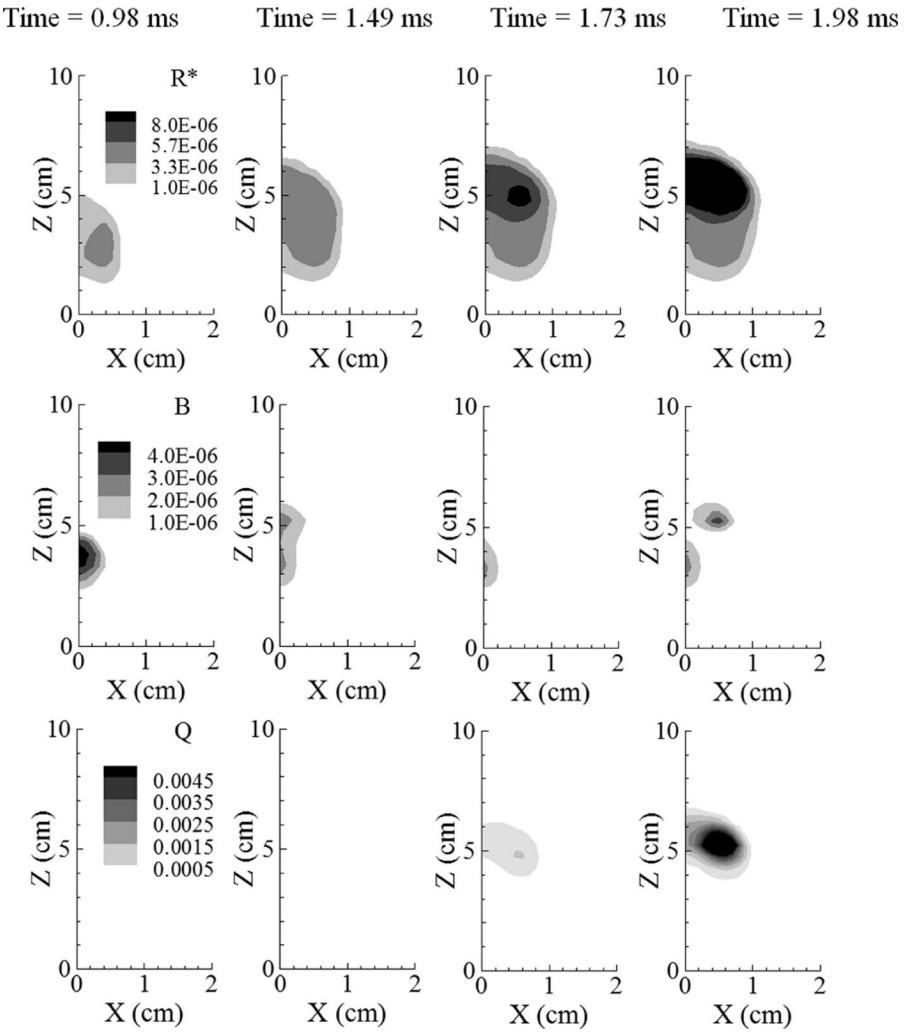

WAVE model compared with other droplet breakup models which are widely used in computer simulation of quasi-steady-state spray dynamics. A similar conclusion is drawn from the predicted and observed SMR of droplets.

The prediction of the total autoignition delay by the Abramzon and Sirignano gas phase model has been compared with the prediction of this delay by a more basic gas phase model, based on a number of simplifying assumptions. It has been shown that the choice of the gas phase model has only a minor effect on the predicted autoignition delay, which can be safely ignored in practical engineering computations. Also, the autoignition delays predicted by the ITC and ETC liquid phase models have been compared. The ITC model is a default one used in the conventional KIVA 2 code. The ETC model is the new model implemented into this code. The implementation of the latter was based on the analytical solution of the heat conduction equation in a spherical droplet applied at each time step (Sazhin et al., 2004b, 2005a, 2005b). It has been pointed out that the difference in the autoignition delay times predicted by the ITC and ETC models is noticeable and needs to be taken into account in practical computations. The application of the ETC model is recommended as a more physical one.

It has been pointed out that the predicted decrease in the autoignition delay with increasing in-cylinder gas pressure in the approximate range 5.5–7 MPa, agrees with experimental observations. However, the predicted values of this delay are up to about 10% less than the experimentally observed ones. This level of agreement between experimental and computational results is considered to be acceptable, remembering the uncertainty about both the data and values of the input parameters in the model. Doubts about the model values of parameters stem primarily from uncertainty about the initial gas temperature (calculated based on the observed in-cylinder gas pressure), injected liquid temperature, and the parameters of the Shell autoignition model. It has been shown that the grid dependence of the results is relatively weak and can be ignored in the analysis.

The detailed analyses of time evolution of various Diesel parameters have been presented. These include gas pressure and temperature, SMR of droplets, mass fractions of various gas components, droplet temperatures

Figure 18 Relative number density, temperature and relative speeds of droplets at four moments in time (the same as in Figures 14–17) and various droplet radii bands. The same values of the initial parameters and models as in Figure 11 were used

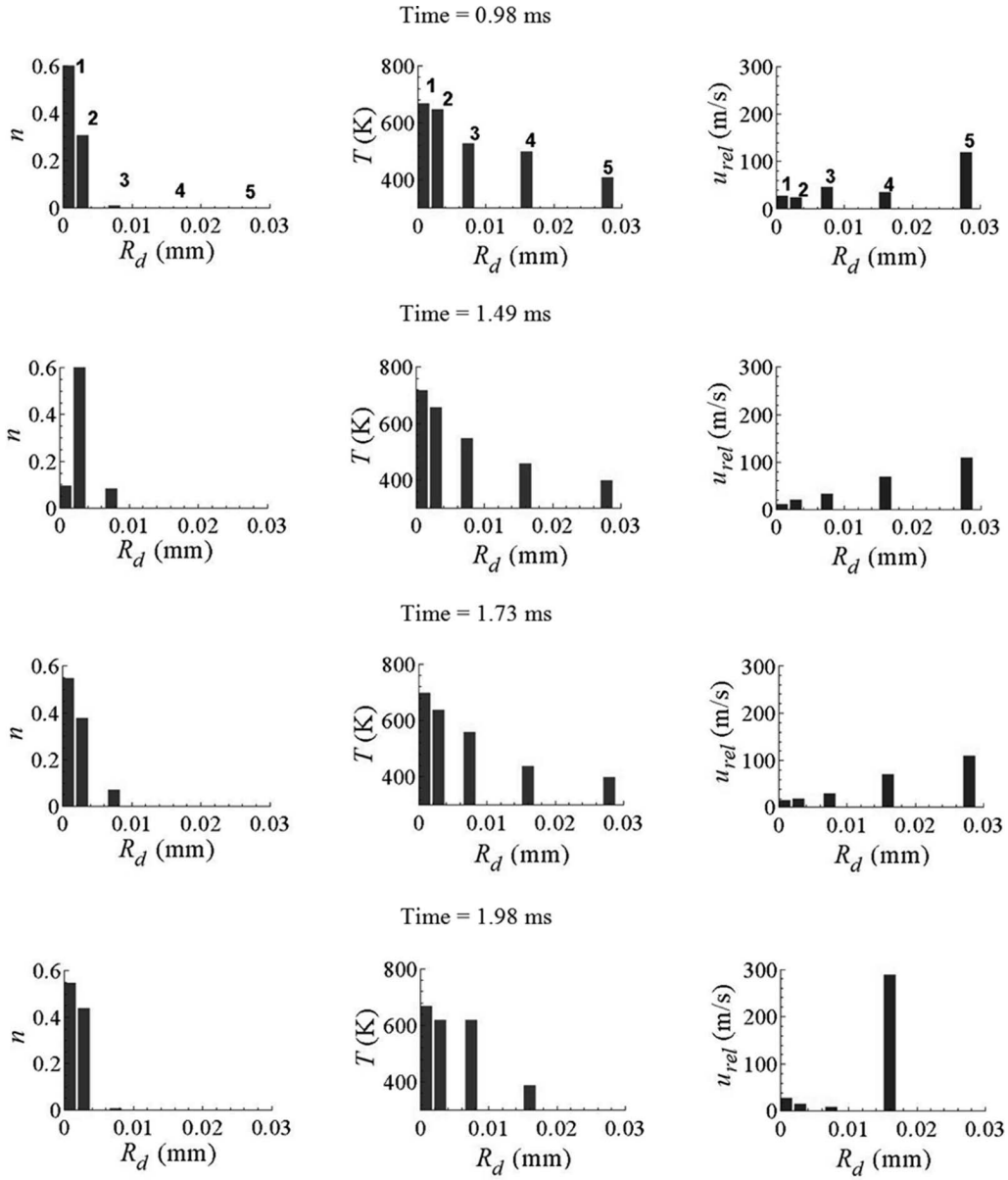

and droplet speeds relative to the ambient gas. The results proved to be consistent with the physical background of the processes involved. In agreement with the previously reported results, it has been shown that autoignition takes place at the periphery of the fuel spray.

Acknowledgment

The authors are grateful to the European Regional Development Fund Franco-British INTERREG IIIa (Project Ref. 162/025/247) and the Indonesian government (TPSDP, Batch III) for financial support of the work on this project. K. Karimi is acknowledged for providing experimental data on transient sprays. Finally, useful discussions with M. Gorokhovski and A. Chtab are gratefully acknowledged.

References

Abramzon, B. and Sazhin, S. (2005) 'Droplet vaporization model in the presence of thermal radiation', *International Journal of Heat and Mass Transfer*, Vol. 48, pp.1868–1873.

Abramzon, B. and Sazhin, S. (2006) 'Convective vaporization of fuel droplets with thermal radiation absorption', *Fuel*, Vol. 85, No. 1, pp.32–46.

Abramzon, B. and Sirignano, W.A. (1989) 'Droplet vaporization model for spray combustion calculations', *International Journal of Heat and Mass Transfer*, Vol. 32, pp.1605–1618.

Amsden, A.A., O'Rourke, P.J. and Butler, T.D. (1989) '*KIVA-II: A Computer Program for Chemically Reactive Flows with Sprays*', Los-Alamos National Laboratory Report No. LA-11560-MS.

Apte, S.V., Gorokhovski, M. and Moin, P. (2003) 'LES of atomizing spray with stochastic modelling of secondary breakup', *International Journal of Multiphase Flow*, Vol. 29, pp.1503–1522.

Arias-Zugasti, M. and Rosner, D.E. (2003) 'Multicomponent fuel droplet vaporization and combustion using spectral theory for a continuous mixture', *Combustion and Flame*, Vol. 135, pp.271–284.

Basevich, V.Ya. (1990) *Handbook of Heat and Mass Transfer*, Gulf Publishing Company, pp.769–819.

Basevich, V.Ya. and Frolov, S.M. (1994) 'A reduced kinetic scheme for autoignition modelling of iso-octane and n-heptane/air mixtures during the induction period for internal combustion engines', *Chemical Physics*, Vol. 13, pp.146–156 (in Russian).

Beale, J.C. and Reitz, R.D. (1999) 'Modeling spray atomization with the Kelvin-Helmholtz/Rayleigh-Taylor hybrid model', *Atomization and Sprays*, Vol. 9, pp.623–650.

Bertoli, C. and na Migliaccio M. (1999) 'A finite conductivity model for diesel spray evaporation computations', *International Journal of Heat and Fluid Flow*, Vol. 20, pp.552–561.

Bird, R.B., Stewart, E.W. and Lightfoot, E.N. (2002) *Transport Phenomena*, 2nd ed., John Wiley & Sons, New York, Chichester.

Carslaw, H.S. and Jaeger, J.C. (1986) *Conduction of Heat in Solids*, Clarendon Press, Oxford.

Cebeci, T. and Smith, A.M.O. (1974) *Analysis of Turbulent Boundary Layers, Series: Applied Mathematics and Mechanics*, Academic Press, NY, USA.

Cooper, F. (1977) 'Heat transfer from a sphere to an infinite medium', *International Journal of Heat and Mass Transfer*, Vol. 20, pp.991–993.

Cuoci, A., Mehl, M., Buzzi-Ferraris, G., Faravelli, T., Manca, D. and Ranzi, E. (2005) 'Autoignition and burning rates of fuel droplets under microgravity', *Combustion and Flame*, Vol. 143, No. 3, pp.211–226.

Crua, C. (2002) *Combustion Processes in a Diesel Engine*, PhD Thesis, University of Brighton. www.crua.net/thesis

Crua, C., Kennaird, D.A., Sazhin, S.S., Heikal, M.R. and Gold, M. (2004) 'Diesel autoignition at elevated in-cylinder pressures', *International Journal of Engine Research*, Vol. 5, No. 4, pp.365–374.

Demoulin, F.X. and Borghi, R. (2003) 'Modeling of turbulent spray combustion with application to diesel like experiment', *Combustion and Flame*, Vol. 129, pp.281–293.

Domann, R. and Hardalupas, Y. (2004) 'Breakup model for accelerating liquid jets', *Proceedings of 42nd AIAA Aerospace Science Meeting and Exhibition*, Reno, Nevada, Paper AIAA-2004-1155.

Dombrovsky, L.A., Sazhin, S.S, Sazhina, E.M, Feng, G., Heikal, M.R., Bardsley, M.E.A. and Mikhalovsky, S.V. (2001) 'Heating and evaporation of semi-transparent diesel fuel droplets in the presence of thermal radiation', *Fuel*, Vol. 80, No. 11, pp.1535–1544.

Faeth, G.M., Hsiang, L-P. and Wu, P-K. (1995) 'Structure and breakup properties of sprays', *International Journal of Multiphase Flow*, Vol. 21, Suppl. 1, pp.99–127.

Flynn, P.F., Durrett, R.P. Hunter, G.L. zur Loye, A.O., Akinyemi, O.C., Dec, J.E. and Westbrook, C.K. (1999) 'Diesel combustion: an integrated view combining laser diagnostics, chemical kinetics, and empirical validation', *SAE Report* 1999-01-0509.

Gorokhovski, M.A. and Saveliev, V.L. (2003) 'Analysis of Kolmogorov's model of breakup and its application into Lagrangian computation of liquid sprays under air-blast atomisation', *Physics of Fluids*, Vol. 15, No. 1, pp.184–192.

Griffiths, J.F. (1995) 'Reduced kinetic models and their application to practical combustion systems', *Progress in Energy and Combustion Science*, Vol. 21, pp.25–107.

Halstead, M.P., Kirsch, L.J. and Quinn, C.P. (1977) 'The autoignition of hydrocarbon fuels at high temperatures and pressures–fitting of a mathematical model', *Combustion and Flame*, Vol. 30, pp.45–60.

Hamosfakidis, V. and Reitz, R.D. (2003) 'Optimization of a hydrocarbon fuel ignition model for two single component surrogates of diesel fuel', *Combustion and Flame*, Vol. 132, pp.433–450.

Hiroyasu, H. and Kadota, T. (1974) 'Fuel droplet size distribution in a diesel combustion chamber', *SAE Paper* 740715.

Kaario, O., Larmi, M. and Tanner, F.X. (2002) 'Non-evaporating liquid spray simulations with the ETAB and WAVE droplet breakup models', *Proceedings of ILASS-Europe*, Zaragoza, Spain, Paper 49.

Karimi, K., Sazhina, E.M., Abdelghaffar, W.A., Crua, C., Heikal, M.R. and Gold M.R. (2006) 'Development in diesel spray characterisation and modelling', *Proceedings of THIESEL-2006*, Valencia, Spain, Session A.1(CD).

Kartashov, E.M. (2001) *Analytical Methods in the Heat Transfer Theory in Solids*, Vysshaya Shkola, Moscow (in Russian).

Kojima, S. (1994) 'Detailed modeling of n-butane autoignition chemistry', *Combustion and Flame*, Vol. 99, pp.87–136.

Kolmogorov, A.N. (1941) 'On the log-normal distribution of particle sizes during the breakup process', *Dokl. Akad. Nauk SSSR*, Vol. 31, p.99.

Kong, S.C., Senecal, P.K. and Reitz, R.D. (1999) 'Developments in spray modelling in diesel and direct-injection gasoline engines', *Oil and Gas Science and Technology Review IFP*, Vol. 54, No. 2, pp.197–204.

Lacoste, J. (2005) *Characteristics of Diesel Sprays at High Temperatures and Pressures*, PhD Thesis, University of Brighton, UK.

Lefebvre, A.H. (1989) *Atomization and Sprays*, Taylor & Francis, Bristol, PA.

Lozano, A., Barreras, F., Hauke, G. and Dopazo, C. (2001) 'Longitudinal instabilities in an air-blasted liquid sheet', *Journal of Fluid Mechanics*, Vol. 437, pp.143–173.

Luikov, A.V. (1968) *Analytical Heat Transfer Theory*, Academic Press, USA.

Miller, R.S., Harstad, K. and Bellan, J. (1998) 'Evaluation of equilibrium and non-equilibrium evaporation models for many-droplet gas-liquid flow simulations', *International Journal of Multophase Flow*, Vol. 24, No. 6, pp.1025–1055.

Minetti, R., Ribaucour, M., Carlier, M., Fittschen, C. and Sochet, L.R. (1994) 'Experimental and modelling study of oxidation and autoignition of butane at high pressure', *Combustion and Flame*, Vol. 96, pp.201–211.

Müller, U.C., Peters, N. and Liñan, A. (1992) 'Global kinetics for n-heptane ignition at high pressures', *Twenty-Fourth Symposium (International) on Combution/The Combustion Institute*, pp.777–784.

Narasimha, R. and Sreenivasan, K.R. (1979) 'Relaminarization of fluid flows', *Advances in Applied Mechanics*, Vol. 19, pp.221–301.

Nijdam, J.J., Guo, B., Fletcher, D.F. and Langrish, T.A.G. (2006) 'Lagrangian and Eulerian models for simulating turbulent dispersion and coalescence of droplets within a spray', *Applied Mathematical Modelling*, Vol. 30, No. 11, pp.1196–1211.

O'Rourke, P.J. (1981) *Collective Drop Effects on Vaporizing Liquid Sprays*, PhD Thesis, Princeton University, Princeton, USA.

O'Rourke, P.J. and Amsden, A.A. (1987) 'The TAB method for numerical calculation of spray droplet breakup', *SAE Paper* 872089.

Patterson, M.A. and Reitz, R.D. (1998) 'Modelling the effects of fuel spray characteristics on diesel engine combustion and emission', *SAE Paper* 980131.

Porter, R., Fairweather, M., Griffiths, J.F., Hughes, K.J. and Tomlin, A.S. (2007) 'Simulated autoignition temperature (AIT) and oxidation of cyclohexane', *Proceedings of the 3rd European Combustion Symposium Chania*, Greece, 11–13 April, paper 3–3.

Ranzi, E., Faravelli, T., Gaffuri, P., Pennati, G.C. and Sogaro, A. (1994) 'A wide range modeling of propane and n-butane oxidation', *Combustion and Flame*, Vol. 100, pp.299–330.

Reitz, R.D. (1987) 'Modelling atomization processes in high-pressure vaporizing sprays', *Atomisation and Spray Technology*, Vol. 3, pp.309–337.

Reitz, R.D. and Rutland, C.J. (1995) 'Development and testing of diesel engine CFD models', *Progress in Energy and Combustion Science*, Vol. 21, No. 2, pp.173–196.

Ribaucour, M., Minetti, R., Sazhina, E.M. and Sazhin, S.S. (2007) 'Autoignition of n-pentane in a rapid compression machine: experiment versus modelling', *Proceedings of the Third European Combustion Meeting ECM 2007*, paper 1–1.

Russel, M.F., Greeves, G. and Guerrassi, N. (2000) 'More torque, less emissions and less noise', *SAE Paper* 2000-01-0942.

Sarre, Ch.K., Kong, S-Ch. and Reitz, R.D. (1999) 'Modelling of the effects of injector nozzle geometry on diesel sprays', *SAE Paper* 1999-01-0912.

Sazhin, S.S. (2006) 'Advanced models of fuel droplet heating and evaporation', *Progress in Energy and Combustion Science*, Vol. 32, No. 2, pp.162–214.

Sazhin, S.S., Sazhina, E.M., Heikal, M.R., Marooney, C. and Mikhalovsky, S.V. (1999) 'The Shell autoignition model: a new mathematical formulation', *Combustion and Flame*, Vol. 117, No. 3, pp.529–540.

Sazhin, S.S., Goldshtein, V. and Heikal, M.R. (2001) 'A transient formulation of Newton's cooling law for spherical bodies', *ASME Journal of Heat Transfer*, Vol. 123, No. 1, pp.63,64.

Sazhin, S.S., Abdelghaffar, W.A., Sazhina, E.M., Mikhalovsky, S.V., Meikle, S.T. and Bai, C. (2004a) 'Radiative heating of semi-transparent diesel fuel droplets', *ASME Journal of Heat Transfer*, Vol. 126, pp.105–109; *Erratum*, Vol. 126, pp.490,491.

Sazhin, S.S., Krutitskii, P.A., Abdelghaffar, W.A., Sazhina, E.M., Mikhalovsky, S.V., Meikle, S.T. and Heikal, M.R. (2004b) 'Transient heating of diesel fuel droplets', *International Journal of Heat and Mass Transfer*, Vol. 47, pp.3327–3340.

Sazhin, S.S., Abdelghaffar, W.A., Krutitskii, P.A., Sazhina, E.M. and Heikal, M.R. (2005a) 'New approaches to numerical modelling of droplet transient heating and evaporation', *International Journal of Heat and Mass Transfer*, Vol. 48, Nos. 19–20, pp.4215–4228.

Sazhin, S.S., Abdelghaffar, W.A., Sazhina, E.M. and Heikal, M.R. (2005b) 'Models for droplet transient heating: effects on droplet evaporation, ignition, and break-up', *International Journal of Thermal Science*, Vol. 44, pp.610–622.

Sazhin, S.S., Kristyadi, T., Abdelghaffar, W.A. and Heikal, M.R. (2006) 'Models for fuel droplet heating and evaporation: comparative analysis', *Fuel*, Vol. 85, Nos. 12–13, pp.1613–1630.

Sazhin, S.S., Krutitskii, P.A., Martynov, S.B., Mason, D., Heikal, M.R. and Sazhina, E.M. (2007a) 'Transient heating of a semitransparent spherical body', *International Journal of Thermal Science*, Vol. 46, No. 5, pp.444–457.

Sazhin, S.S., Kristyadi T., Abdelghaffar, W.A., Begg, S., Heikal, M.R., Mikhalovsky, S.V., Meikle S.T. and Al-Hanbali, O. (2007b) 'Approximate analysis of thermal radiation absorption in fuel droplets', *ASME Journal of Heat Transfer*, Vol. 129, pp.1246–1255.

Sazhina, E.M., Sazhin, S.S., Heikal, M.R. and Marooney, C. (1999) 'The Shell autoignition model: application to gasoline and diesel fuels', *Fuel*, Vol. 78, No. 4, pp.389–401.

Sazhina, E.M., Sazhin, S.S., Heikal, M.R., Babushok, V.I. and Johns, R. (2000) 'A detailed modelling of the spray ignition process in diesel engines', *Combustion Science and Technology*, Vol. 160, pp.317–344.

Schugger, C., Meingast, U. and Renz, U. (2000) 'Time-resolved velocity measurements in the primary breakup zone of a high pressure diesel injection nozzle', *Proceedings of ILASS-Europe*, Darmstadt, Germany.

Stauch, R., Lipp, S. and U. Maas, U. (2006) 'Detailed numerical simulations of the autoignition of single n-heptane droplets in air', *Combustion and Flame*, Vol. 145, No. 3, pp.533–542.

Stiesch, G. (2003) *Modelling Engine Sprays and Combustion Processes*, Springer, Berlin, London, UK.

Tanner, F.X. (2004) 'Development and validation of a cascade atomization and drop breakup model for high-velocity dense sprays', *Atomization and Sprays*, Vol. 14, pp.211–242.

Wang, Y. and Rutland, C.J. (2007) 'Direct numerical simulation of ignition in turbulent n-heptane liquid-fuel spray jets', *Combustion and Flame*, Vol. 149, No. 4, pp.353–365.

Wong, S-C, Liao, X.X and Yang, J.R. (1997) 'A simplified theory of the ignition of single droplets under forced convection', *Combustion and Flame*, Vol. 110, No. 3, pp.319–334.

Wright, Y.M., De Paola, G., Boulouchos, K. and Mastorakos, E. (2005) 'Simulations of spray autoignition and flame establishment with two-dimensional CMC', *Combustion and Flame*, Vol. 143, No. 4, pp.402–419.

Yang, J-R. and Wong, S-C. (2003) 'On the suppression of negative temperature coefficient (NTC) in autoignition of n-heptane droplets', *Combustion and Flame*, Vol. 132, No. 3, pp.475–491.

Zhou, P., Zhou, S. and Clelland, D. (2006) 'A modified quasi-dimensional multi-zone combustion model for direct injection diesels', *International Journal of Engine Research*, Vol. 7, No. 4, pp.335–345.